iScience

CellPress
OPEN ACCESS

Article

A genetically targeted ion sensor reveals distinct seizure-related chloride and pH dynamics in GABAergic interneuron populations

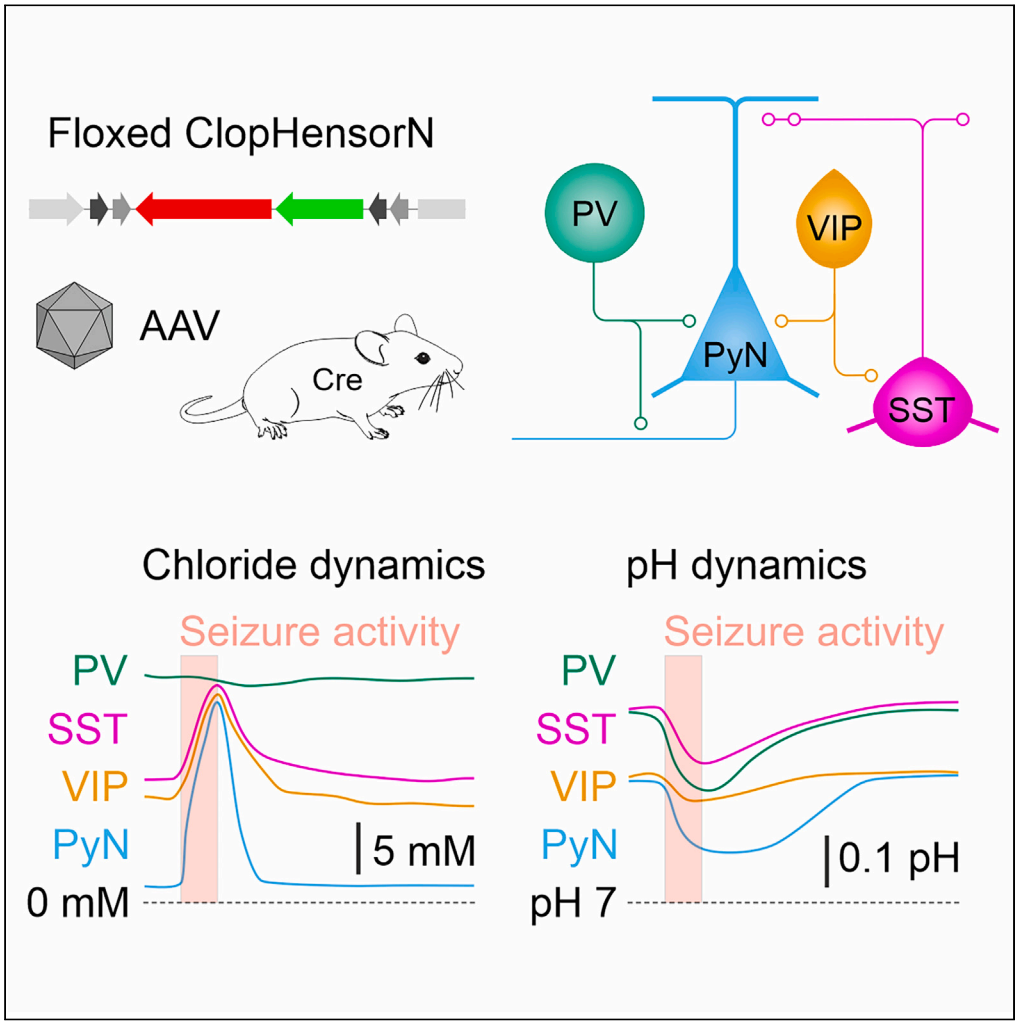

Alexandru Călin, Tatiana Waseem, Joseph V. Raimondo, Sarah E. Newey, Colin J. Akerman

colin.akerman@pharm.ox.ac.uk

Highlights

An optical tool to dissociate chloride and pH in genetically defined cell subtypes

GABAergic interneuron subtypes exhibit distinct resting and dynamic chloride levels

Subtypes converge upon an elevated chloride level during epileptiform activity

Interneuron subtypes exhibit different acidification during epileptiform activity

Călin et al., iScience 26, 106363
April 21, 2023
https://doi.org/10.1016/j.isci.2023.106363

iScience

CellPress
OPEN ACCESS

Article

A genetically targeted ion sensor reveals distinct seizure-related chloride and pH dynamics in GABAergic interneuron populations

Alexandru Călin,[1] Tatiana Waseem,[1] Joseph V. Raimondo,[2] Sarah E. Newey,[1] and Colin J. Akerman[1,3,*]

SUMMARY

Intracellular chloride and pH play fundamental roles in determining a neuron's synaptic inhibition and excitability. Yet it has been difficult to measure changes in these ions during periods of heightened network activity, such as occur in epilepsy. Here we develop a version of the fluorescent reporter, ClopHensorN, to enable simultaneous quantification of chloride and pH in genetically defined neurons during epileptiform activity. We compare pyramidal neurons to the major GABAergic interneuron subtypes in the mouse hippocampus, which express parvalbumin (PV), somatostatin (SST), or vasoactive intestinal polypeptide (VIP). Interneuron populations exhibit higher baseline chloride, with PV interneurons exhibiting the highest levels. During an epileptiform discharge, however, all subtypes converge upon a common elevated chloride level. Concurrent with these dynamics, epileptiform activity leads to different degrees of intracellular acidification, which reflect baseline pH. Thus, a new optical tool for dissociating chloride and pH reveals neuron-specific ion dynamics during heightened network activity.

INTRODUCTION

Intracellular chloride levels are fundamental to normal brain function. Chloride levels establish the reversal potential for $GABA_A$ receptors (E_{GABA_A}), which determines the post-synaptic effects of GABA-mediated synaptic transmission. As intracellular chloride levels are significantly lower than extracellular levels, the opening of $GABA_A$ receptors ($GABA_A$Rs) is typically associated with chloride influx and hyperpolarizing effects upon the membrane. During intense activation of $GABA_A$Rs however, chloride influxes can exceed regulatory mechanisms, which leads to an increase in intracellular chloride levels and a reduction in the transmembrane chloride gradient.[1–6] For example, intense $GABA_A$R activation during an epileptiform discharge (ED) causes depolarizing shifts in the E_{GABA_A} of hippocampal pyramidal neurons,[6–10] which can switch the action of $GABA_A$Rs, such that they begin to promote rather than oppose epileptiform activity.[10–14]

Although previous studies have tended to focus on chloride regulation in excitatory neurons, a number of electrophysiological studies have suggested that chloride regulation may differ in GABAergic interneurons. For example, GABA-mediated inputs to CA3 hippocampal stratum lucidum interneurons tend to be shunting, consistent with a relatively high intracellular chloride level.[15] Similar observations, also consistent with relatively high chloride levels, have been reported in interneurons from other brain regions, including the dorsal cochlear nucleus,[16] cerebellum,[17] basolateral amygdala, parietal cortex, perirhinal cortex,[18] interneurons of the CA1 region of the hippocampus,[19,20] dentate gyrus,[21,22] and stratum radiatum.[23] These studies used current fluxes through transmembrane receptors to infer chloride levels under resting conditions, but such electrophysiological measurements are compromised during epileptiform activity due to the dramatic changes in a neuron's biophysical properties and effects upon the chloride-permeable receptors.

Developments in chloride imaging now offer the opportunity to make direct measurements of intracellular chloride levels. For example, genetically encoded chloride reporters such as Clomeleon[24] and Cl-sensor[25] afforded the first ratiometric chloride measurements from neurons. More recently, the development of ClopHensor[26] has enabled simultaneous ratiometric measurements of both chloride and pH. Importantly, this feature of ClopHensor avoids the confound of earlier reporters, which are sensitive to both chloride

[1]Department of Pharmacology, University of Oxford, Oxford OX1 3QT, UK

[2]Division of Cell Biology, Department of Human Biology, Neuroscience Institute and Institute of Infectious Disease and Molecular Medicine, Faculty of Health Sciences, University of Cape Town, Cape Town 7925, South Africa

[3]Lead contact

*Correspondence: colin.akerman@pharm.ox.ac.uk

https://doi.org/10.1016/j.isci.2023.106363

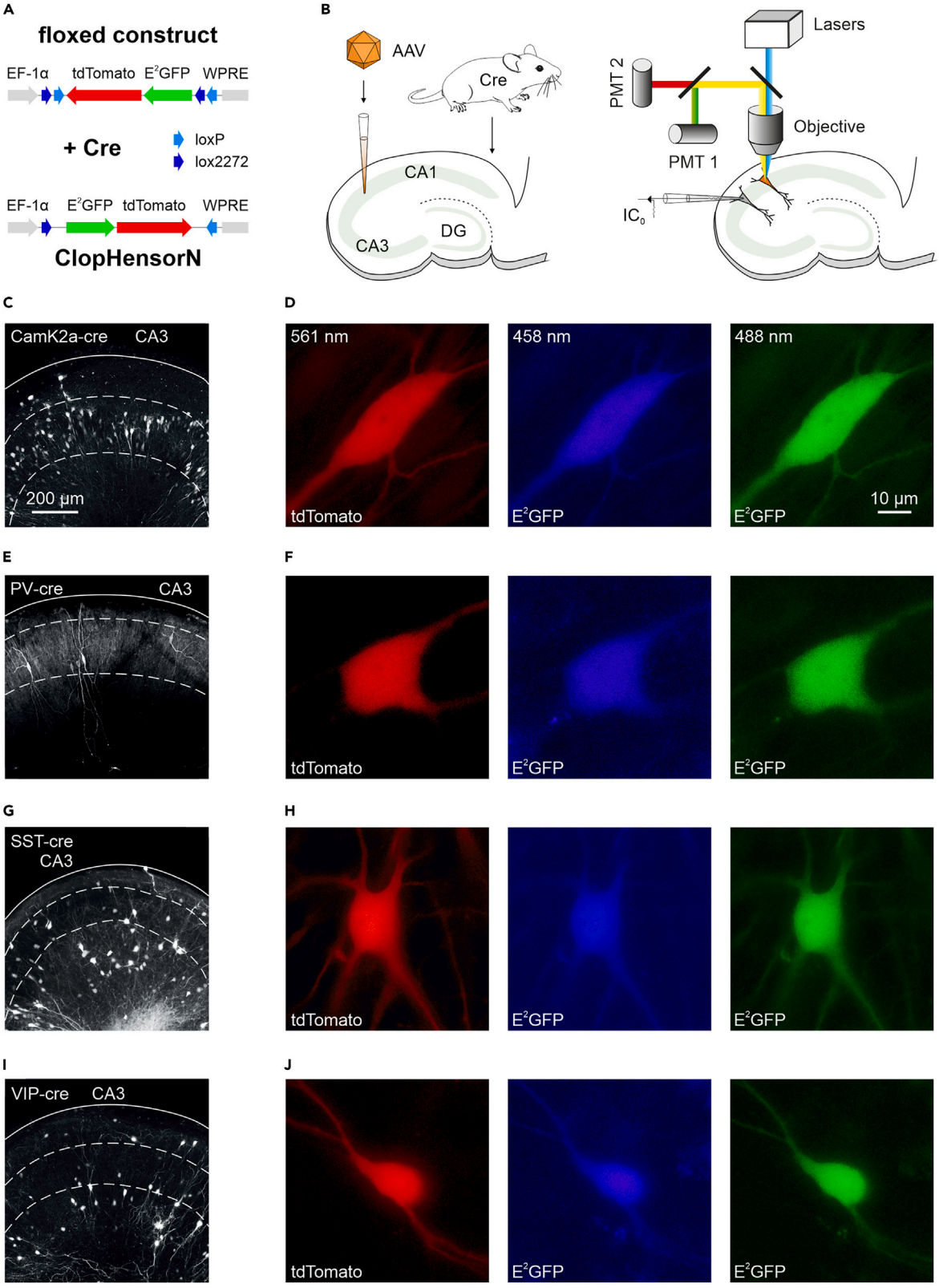
A
floxed construct
EF-1α tdTomato E²GFP WPRE
+ Cre
loxP
lox2272
EF-1α E²GFP tdTomato WPRE
ClopHensorN
B
AAV
Cre
CA1
DG
CA3
Lasers
PMT 2
Objective
PMT 1
IC0
C
CamK2a-cre CA3
200 μm
D
561 nm
458 nm
488 nm
tdTomato
E²GFP
E²GFP
10 μm
E
PV-cre CA3
F
tdTomato
E²GFP
E²GFP
G
SST-cre
CA3
H
tdTomato
E²GFP
E²GFP
I
VIP-cre CA3
J
tdTomato
E²GFP
E²GFP

Figure 1. Cre-dependent ClopHensorN for targeting expression to genetically defined neuronal subtypes

(A) The Cre-dependent ClopHensorN construct contained the inverted genetic sequence for the E^2GFP-tdTomato fusion protein, flanked by *loxP* and *lox2272* sites. The construct utilizes an elongation factor 1α promoter (EF-1α) and a WPRE to enhance expression. Cre recombinase catalyses the recombination of the floxed sequence, which allows for transcription of ClopHensorN.

(B) High-titer AAV carrying the Cre-dependent ClopHensorN was delivered to organotypic hippocampal brain slices from Cre-expressing mice and, after three weeks in culture, ClopHensorN-expressing neurons were imaged using confocal microscopy. Simultaneous electrophysiological data were acquired via patch-clamp recordings from a nearby pyramidal neuron in current-clamp mode (IC_0).

(C) Hippocampal slice from a CamK2a-Cre mouse containing ClopHensorN-expressing pyramidal neurons. Continuous white lines indicate the slice edge and dashed white lines delineate the pyramidal cell layer.

(D) ClopHensorN signal from a representative pyramidal neuron, in which the tdTomato protein was excited at 561 nm (left), and the E^2GFP protein was excited at 458 nm (middle), and 488 nm (right).

(E and F) Equivalent images for a slice from a PV-Cre mouse (E) and the ClopHensorN signal from a representative PV interneuron (F).

(G and H) Equivalent images for a slice from an SST-Cre mouse (G) and the ClopHensorN signal from a representative SST interneuron (H).

(I and J) Equivalent images for a slice from a VIP-Cre mouse (I) and the ClopHensorN signal from a representative VIP interneuron (J).

ions and protons, but unable to distinguish these ions. This is particularly relevant in the context of epileptiform activity, where the levels of multiple ion species are known to change.[27,28] For instance, previous imaging studies have shown that excitatory hippocampal neurons rapidly accumulate intracellular chloride around the onset of an ED,[9,27,28] consistent with depolarizing shifts in the E_{GABA_A}. However, these chloride dynamics associated with epileptiform activity coincide with other changes in ion concentrations, including increases in extracellular potassium[29–31] and increases in intracellular protons (i.e. acidification).[27,32]

Here we use ClopHensorN—a version of ClopHensor that has been optimized for the nervous system[27]—in order to dissociate chloride and proton dynamics in different neuronal subtypes of the hippocampus. To this end, we develop and characterize a floxed version of ClopHensorN, which we target in a Cre-dependent manner to pyramidal neurons, and also parvalbumin (PV), somatostatin (SST), and vasoactive intestinal polypeptide (VIP) expressing interneurons of the mouse hippocampus. This reveals neuronal subtype differences in the baseline and dynamic intracellular chloride and pH levels associated with epileptiform activity.

RESULTS

A Cre-dependent ClopHensorN for measuring intracellular chloride and pH in genetically defined cell types

To image chloride and pH in genetically defined neuronal subtypes we generated a double-floxed version of ClopHensorN, which would enable us to take advantage of the Cre-lox system (Figure 1A). The floxed sequence in the construct is permanently inverted in the presence of Cre recombinase, and ClopHensorN expression is under the control of the EF-1α promoter and enhanced via a WPRE and polyA sequence (Figure 1A). High titer AAVs were used to deliver floxed ClopHensorN to organotypic hippocampal brain slices generated from different transgenic mouse lines expressing Cre recombinase under neuronal subtype-specific promoters (Figure 1B). The hippocampal organotypic slice represents an experimentally accessible model of epileptogenesis,[33–35] which retains many features of the hippocampal circuit, including appropriate distributions of interneurons and distinct subcellular targeting of pyramidal neurons.[34,36–38] Approximately three weeks after transduction, ClopHensorN-expressing neurons were imaged using confocal microscopy and could be combined with simultaneous electrophysiological recordings of network activity, by performing whole-cell patch-clamp recordings from a nearby pyramidal neuron (Figure 1B).

Pyramidal neurons, the principal excitatory neurons of the hippocampus, were successfully targeted in brain slices from CamK2a-cre mice, resulting in a pattern of ClopHensorN expression typical for excitatory neurons along the pyramidal layer of the hippocampal brain slice (Figure 1C), with neurons showing robust expression of both tdTomato and E^2GFP (Figure 1D). In addition to pyramidal neurons, we successfully targeted three of the major interneuron subtypes in the hippocampus: PV-, SST-, and VIP-expressing interneurons. Transducing brain slices from PV-Cre mice, resulted in ClopHensorN expression within the soma and processes of PV interneurons that are restricted to the pyramidal cell layer (Figures 1E and 1F), consistent with previous work.[39,40] Transducing brain slices from SST-Cre mice resulted in ClopHensorN expression in the soma and processes of SST interneurons that are located within stratum oriens and lacunosum-moleculare (Figures 1G and 1H), consistent with previous work.[34] Finally,

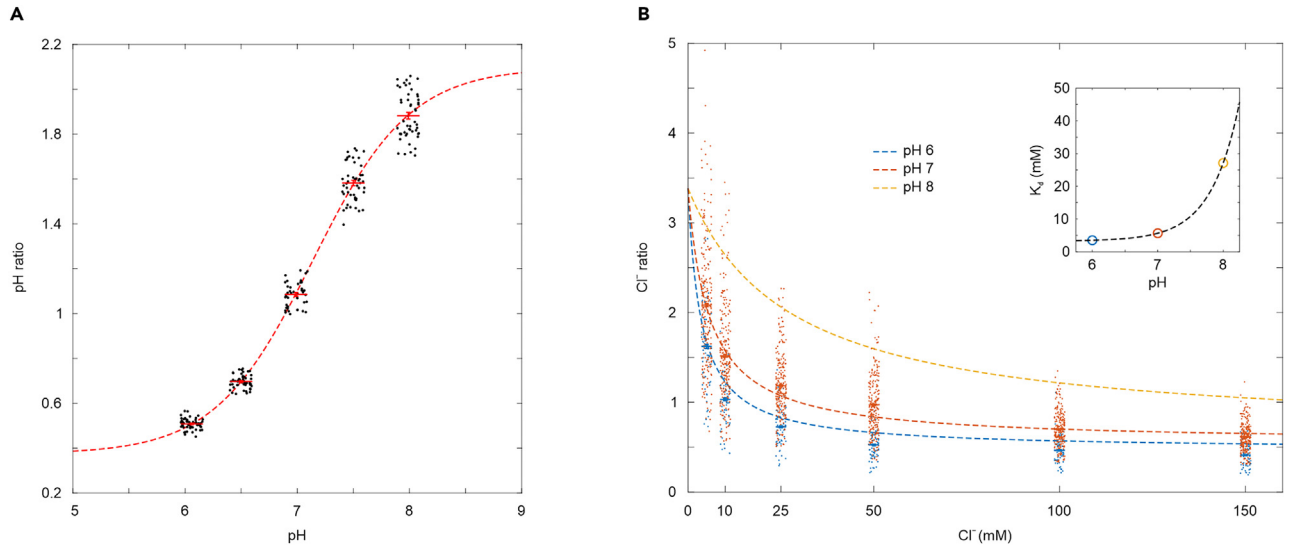

Figure 2. ClopHensorN calibration

(A) Calibration curves relating the pH sensitive ratio (F_{488}/F_{458}) of ClopHensorN to intracellular pH. Intracellular pH was systematically varied by controlling the extracellular pH in the presence of an ionophore cocktail. Data was fit using established equations[27,44] and pK_a was estimated to be 7.14 (CI [7.1–7.17]). N = 40–60 cells at each pH value. Horizontal lines indicate mean, error bars indicate SEM, and dots indicate individual cells.

(B) Calibration curves relating the chloride sensitive fluorescence ratio (F_{458}/F_{561}) to intracellular chloride concentration. Intracellular chloride was manipulated by changing the extracellular chloride in the presence of an ionophore cocktail. Data collected at pH 6 and 7 were fit using established equations as in "A", and used to infer the relationship at pH 8. K_d was estimated to be 3.51 mM at pH 6, 5.66 mM at pH 7, and 27.12 mM at pH 8 (inset). N = 66 and 232 cells at each chloride value for pH 6 and 7, respectively. Horizontal lines indicate mean, error bars indicate SEM, and dots indicate individual cells.

transducing brain slices from VIP-Cre mice, resulted in ClopHensorN expression in VIP interneuron soma and processes located within stratum radiatum, lacunosum-moleculare, pyramidale, and oriens[41,42] (Figures 1I and 1J).

To perform ratiometric measurements of pH and chloride concentration, ClopHensorN and the imaging system were calibrated using established methods.[26,27,43] This involved collapsing the transmembrane gradients for the two ion species and systematically changing pH and chloride in the extracellular and intracellular environment (see STAR Methods). The pH ratio of ClopHensorN-expressing cells—the ratio of emitted fluorescence from the E^2GFP protein when excited sequentially at 458 nm and 488 nm (F_{488}/F_{458})—was found to depend on intracellular pH with a pK_a of 7.14 (95% confidence interval (CI) [7.1–7.17]; Figure 2A); which is comparable to previous work.[27] R_A was 0.37 and R_B was 2.1. Meanwhile, the chloride ratio—the ratio of emitted fluorescence from the tdTomato and E^2GFP proteins when excited sequentially at 561 nm and 458 nm, respectively (F_{458}/F_{561})—was shown to depend on the intracellular chloride concentration with an average K_d of 8.73 mM around the physiological 7.2–7.5 intracellular pH range, ${}^1K_d^{Cl^-}$ of 3.28, and R_{free} of 3.38 (Figure 2B).

Using these calibration curves, ClopHensorN signals were converted into estimates of intracellular chloride and pH for the different neuronal subtypes imaged in organotypic hippocampal brain slices. Initially, we compared the chloride and pH levels under baseline conditions, by restricting the ClopHensorN measurements to periods when the network activity was quiescent, as determined from whole-cell patch-clamp recordings from a nearby pyramidal neuron (Figure 1B; see STAR Methods). Baseline intracellular chloride concentrations were found to vary significantly across neuronal subtypes ($p = 0.0002$, $\chi^2_{(3)} = 19.43$, Kruskal-Wallis test; Figure 3A). Consistent with previous work that either inferred intracellular chloride from electrophysiological recordings[10,20,45] or made direct estimates from imaging methods,[9,27,28,46] CamK2a pyramidal neurons were found to exhibit a low median baseline chloride concentration of 2.0 mM (interquartile range (IQR) [−0.8 to 9.6 mM]). In contrast, interneuron populations tended to exhibit higher baseline chloride values, with PV interneurons exhibiting the highest median baseline somatic chloride concentration at 22.1 mM (IQR [11.8 to 49.5 mM]), which was significantly higher than pyramidal neurons ($p < 0.0001$; Dunn's post-hoc test). This observation is consistent with previous electrophysiological

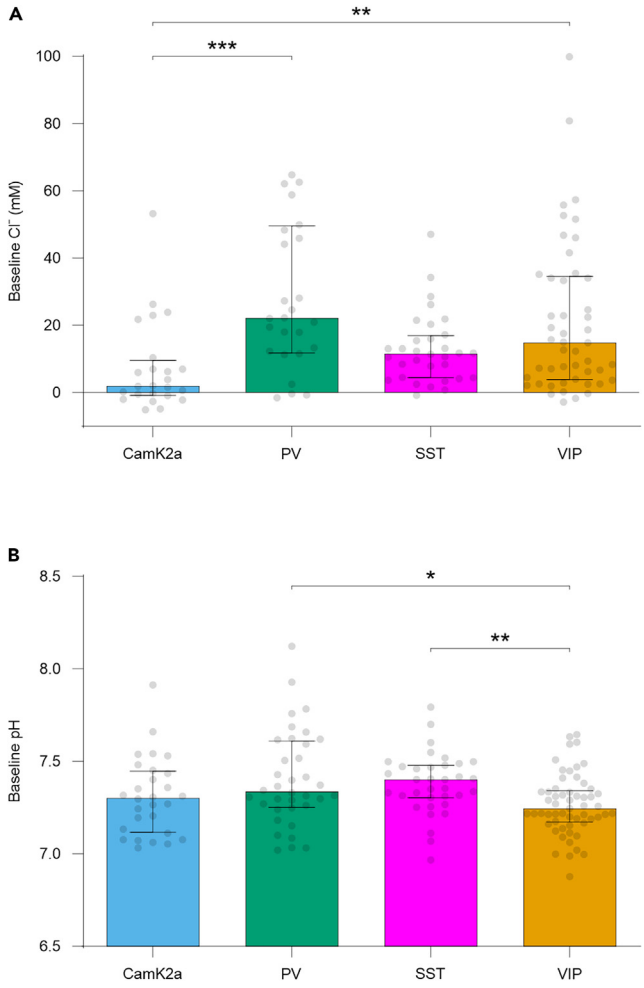

Figure 3. Neuronal subtypes exhibit different baseline intracellular chloride and pH values

(A) Intracellular chloride varies across neuronal subtypes, with PV interneurons and VIP interneurons exhibiting higher baseline chloride than CamK2a pyramidal neurons ($\chi^2_{(3)}$ = 19.43, p = 0.0002, Kruskal-Wallis test, followed by post-hoc Dunn's multiple comparisons tests; CamK2a vs PV, p = 0.0001; CamK2a vs SST, p = 0.1493; CamK2a vs VIP, p = 0.0052; PV vs SST, p = 0.1521; PV vs VIP, p = 0.8035; SST vs VIP, p > 0.999). N = 24, 28, 32 and 49 neurons from 15, 26, 12 and 26 slices for CamK2a, PV, SST and VIP, respectively. Y axis is limited to 100 mM for plotting purposes. Bars and lines indicate median and IQR, dots indicate individual neurons.

(B) Baseline intracellular pH varies across neuronal subtypes. No interneuron subtype was different from CamK2a pyramidal neurons, but within the interneuron subtypes, VIP interneurons exhibited a more acidic baseline pH than PV or SST interneurons ($\chi^2_{(3)}$ = 13.5, p = 0.0037, Kruskal-Wallis test, followed by post-hoc Dunn's multiple comparisons tests; CamK2a vs PV, p = 0.8375; CamK2a vs SST, p = 0.3606; CamK2a vs VIP, p > 0.9999; PV vs SST, p > 0.9999; PV vs VIP, p = 0.0353; SST vs VIP, p = 0.0078). N = 28, 36, 35 and 57 neurons from 15, 26, 12 and 26 slices for CamK2a, PV, SST and VIP, respectively. Bars and lines indicate median and IQR, dots indicate individual neurons. * indicates p < 0.05, ** indicates p < 0.01, *** indicates p < 0.001.

measurements of resting E_{GABA_A} in fast-spiking PV interneurons and pyramidal neurons.[18,20,21] VIP interneurons exhibited a median baseline somatic chloride concentration of 14.8 mM (IQR [3.9 to 34.6 mM]), which was also higher than pyramidal neurons (p = 0.0052; Dunn's post-hoc test). Finally, SST interneurons exhibited a median baseline somatic chloride concentration of 11.6 mM (IQR [4.5 to 16.9 mM]), which was not statistically different from pyramidal neurons (p = 0.149; Dunn's post-hoc test). Using the standard deviation of the pyramidal neuron's membrane potential as a readout of overall slice activity, no cell type exhibited a significant correlation between baseline slice activity and intracellular chloride concentration (CamK2a, r^2 = 0.01, $F_{(1,86)}$ = 1.11, p = 0.2956; PV, r^2 = 0.001, $F_{(1,48)}$ = 0.07, p = 0.7993; SST, r^2 = 0.002, $F_{(1,94)}$ = 0.16, p = 0.6907; VIP, r^2 = 0.02, $F_{(1,122)}$ = 2.29, p = 0.1326; F tests).

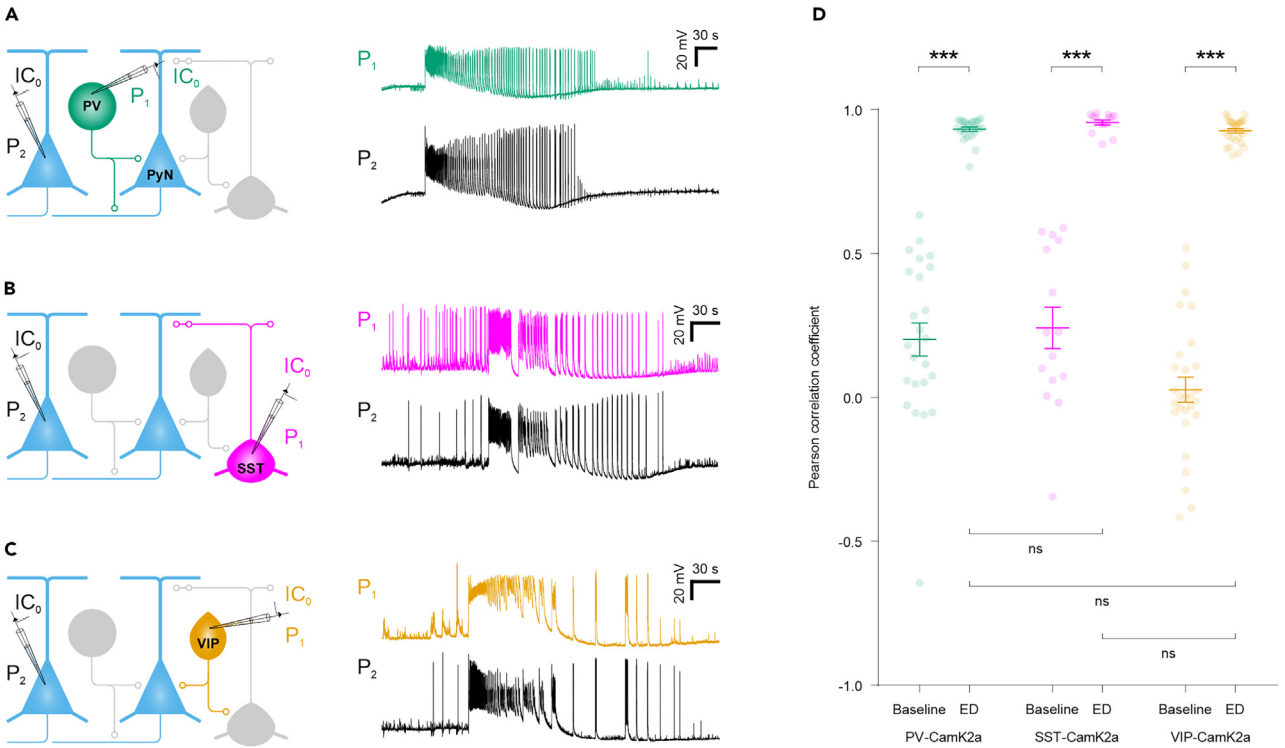

Figure 4. The activity of GABAergic interneuron subtypes and pyramidal neurons is highly correlated during epileptiform activity

(A) Cartoon illustrating simultaneous current clamp recordings from a PV interneuron (Pipette 1, P_1) and a nearby pyramidal neuron (P_2; left). Representative traces (right) from a PV interneuron (top) and a pyramidal neuron (bottom) pair during an ED.

(B) Equivalent cartoon (left) and example traces (right) from an SST interneuron (top) and a pyramidal neuron (bottom) pair during an ED.

(C) Equivalent cartoon (left) and example traces (right) from a VIP interneuron (top) and a pyramidal neuron (bottom) pair during an ED.

(D) During EDs, the activity of PV (N = 24 EDs from 8 neuronal pairs in 8 slices), SST (N = 15 EDs from 8 neuronal pairs in 3 slices) and VIP (N = 28 EDs from 9 neuronal pairs in 6 slices) interneurons was highly correlated with the activity of nearby pyramidal neurons (interaction between neuron pair type and time window: $F_{(2,64)} = 3.771$, $p = 0.0283$, repeated measures two-way ANOVA followed by Sidak's post-hoc multiple comparisons of baseline vs ED: PV-CamK2a, $p < 0.0001$; SST-CamK2a, $p < 0.0001$; VIP-CamK2a, $p < 0.0001$). Lines indicate median and IQR, dots indicate individual EDs. The degree of correlation with the pyramidal neuron's activity was not different across the interneuron subtypes during EDs (Sidak's post-hoc multiple comparisons, $p > 0.05$). *** indicates $p < 0.001$.

Baseline pH values showed subtle but statistically significant differences across the neuronal subtypes ($p = 0.0037$, $\chi^2_{(3)} = 13.5$, Kruskal-Wallis test; Figure 3B), with the largest difference between subtypes equating to a difference of 0.15 pH units. Median baseline pH in CamK2a pyramidal neurons was 7.3 (IQR [7.12 to 7.45]), which was consistent with previous reported values for pyramidal neurons.[27,46,47,48] Unlike chloride, the baseline pH of pyramidal neurons was not statistically different from the pH in any of the interneuron subtypes. Among the interneuron subtypes however, VIP interneurons exhibited a median baseline pH of 7.25 (IQR [7.17 to 7.34]), which was more acidic than the PV interneuron median baseline pH of 7.34 (IQR [7.25 to 7.6]) ($p = 0.0353$; Dunn's post-hoc test) or the SST interneuron median baseline pH of 7.4 (IQR [7.31 to 7.48]) ($p = 0.0078$; Dunn's post-hoc test).

Monitoring chloride and pH dynamics in neuronal subtypes during epileptiform activity

To investigate chloride and pH dynamics during epileptiform activity, we made use of the fact that organotypic hippocampal brain slices readily exhibit EDs[33,49] (see the STAR Methods section). Previous studies have shown that these EDs are characterized by regular, large ictal-like discharges, which comprise hypersynchronous activity across the pyramidal neuron network, and are interspersed by relatively quiescent periods.[10,27,50] To establish that the different interneuron populations also exhibit synchronous activity during EDs, we performed dual whole cell current-clamp recordings from pairs of neurons comprising a specific interneuron and a nearby pyramidal neuron (Figures 4A–4C). During EDs, the membrane potential of PV interneurons (Pearson's coefficient of 0.93 ± 0.01; Figure 4A), SST interneurons (Pearson's coefficient of

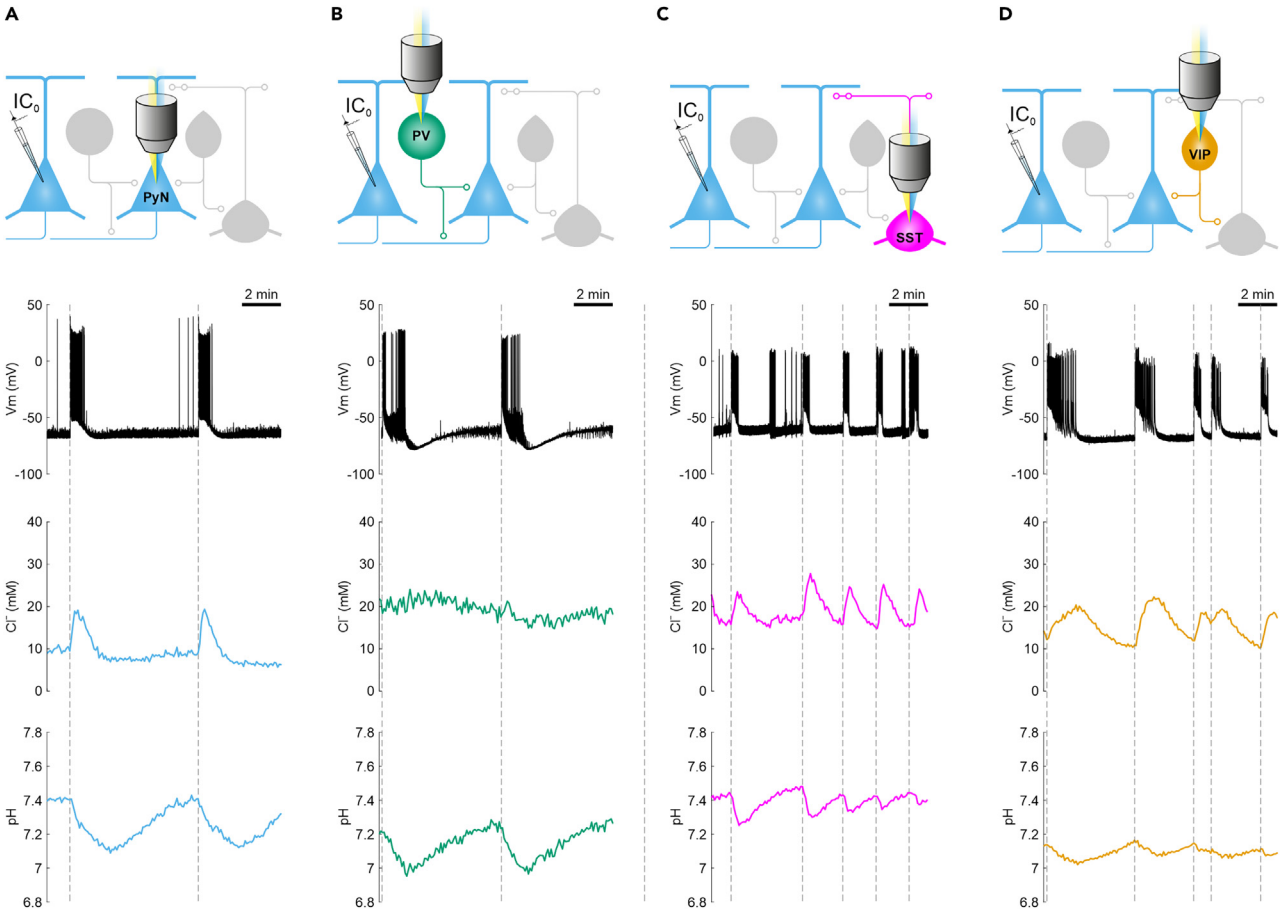

Figure 5. Monitoring chloride and pH dynamics in different neuronal subtypes during epileptiform activity

(A) Cartoon of the experimental setup (top panel) and representative data for a CamK2a pyramidal neuron (bottom three panels). Network activity was always monitored via a current-clamp recording from a nearby pyramidal cell (black trace, second panel), while intracellular chloride dynamics (third panel) and pH dynamics (bottom panel) were determined for a ClopHensorN-expressing CamK2a pyramidal neuron. Data are shown for a representative 10 min period of the recording. Vertical dashed lines mark the start of EDs.

(B) Equivalent cartoon and example data for a PV interneuron.

(C) Equivalent cartoon and example data for an SST interneuron.

(D) Equivalent cartoon and example data for a VIP interneuron.

0.96 ± 0.01; Figure 4B), and VIP interneurons (Pearson's coefficient of 0.93 ± 0.01; Figure 4C) were all highly correlated with the membrane potential of nearby pyramidal neurons. Furthermore, the degree of synchrony during EDs was not different across the three neuron pair types (Figure 4D). These data confirmed that all of the neuronal subtypes of interest exhibit highly correlated activity during the EDs and that recordings from pyramidal neurons are therefore a good way to monitor network activity during epileptiform activity.

To quantify chloride and pH dynamics during EDs, we combined whole-cell patch-clamp recording from a pyramidal neuron, with floxed ClopHensorN imaging from a nearby neuron of a defined subtype (Figure 5). This allowed us to acquire chloride concentration and pH measurements, while monitoring network activity in a manner that did not perturb the physiology of the imaged neuron. The electrophysiological recordings also enabled us to detect the onset and duration of the EDs with an automated algorithm (see STAR Methods). We found that EDs were associated with marked transients in intracellular pH and chloride concentration across the different neuronal subtypes, as shown in the example recordings in Figure 5. Pyramidal neurons (Figure 5A) and the different interneuron subtypes (Figures 5B–5D) exhibited different degrees of change in both their intracellular chloride concentrations and pH levels during EDs.

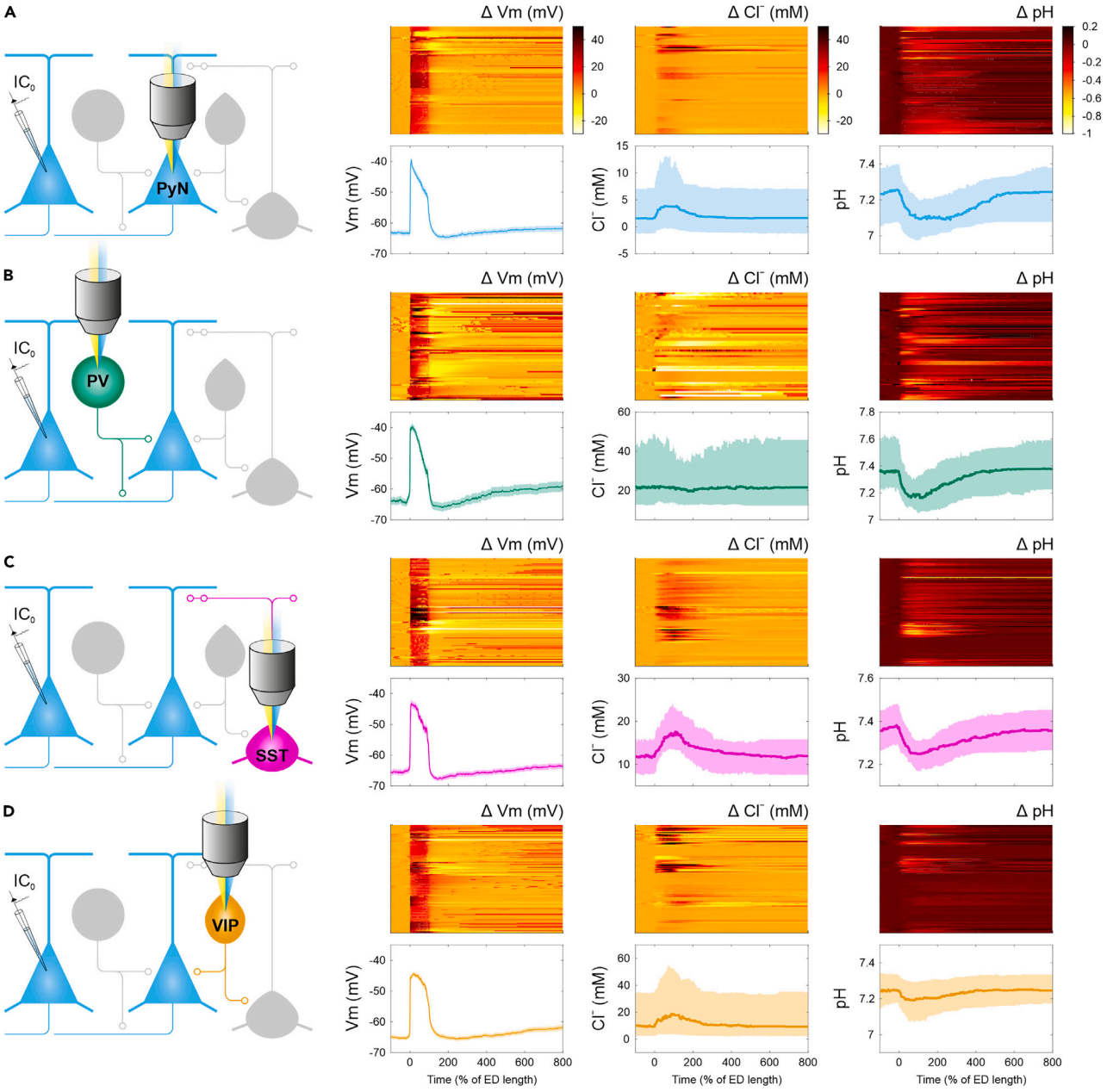

Figure 6. Neuronal subtypes exhibit distinct chloride and pH dynamics during an ED

(A) Cartoon (left) of the experimental setup for a CamK2a pyramidal neuron. Heat maps (right, upper row) show the membrane potential dynamics (Δ Vm), chloride dynamics (Δ Cl^-), and pH dynamics (Δ pH) during all EDs for CamK2a neurons, relative to normalized ED length on the x axis. ED start is at 0% and ED end is at 100%. Plots (right, lower row) show the mean absolute membrane potential, and the median absolute chloride and pH across all CamK2a EDs, using the same x axis timescale. Shading depicts SEM for membrane potential and IQR for chloride and pH. N = 93 EDs from 23 CamK2a neurons in 15 slices.

(B) Equivalent cartoon and data for all EDs in PV interneurons (N = 60 EDs from 28 PV interneurons in 26 slices).

(C) Equivalent cartoon and data for all EDs in SST interneurons (N = 88 EDs from 32 SST interneurons in 12 slices).

(D) Equivalent cartoon and data for all EDs in VIP interneurons (N = 123 EDs from 44 VIP interneurons in 26 slices).

Neuronal subtypes exhibit distinct chloride and pH dynamics during epileptiform activity

We used the above experimental setup to conduct recordings from a population of CamK2a pyramidal neurons, and PV, SST, and VIP interneurons. The resulting data are plotted in different forms in Figure 6 and Figure 7. First, we compared the chloride and pH dynamics during individual EDs for each of the

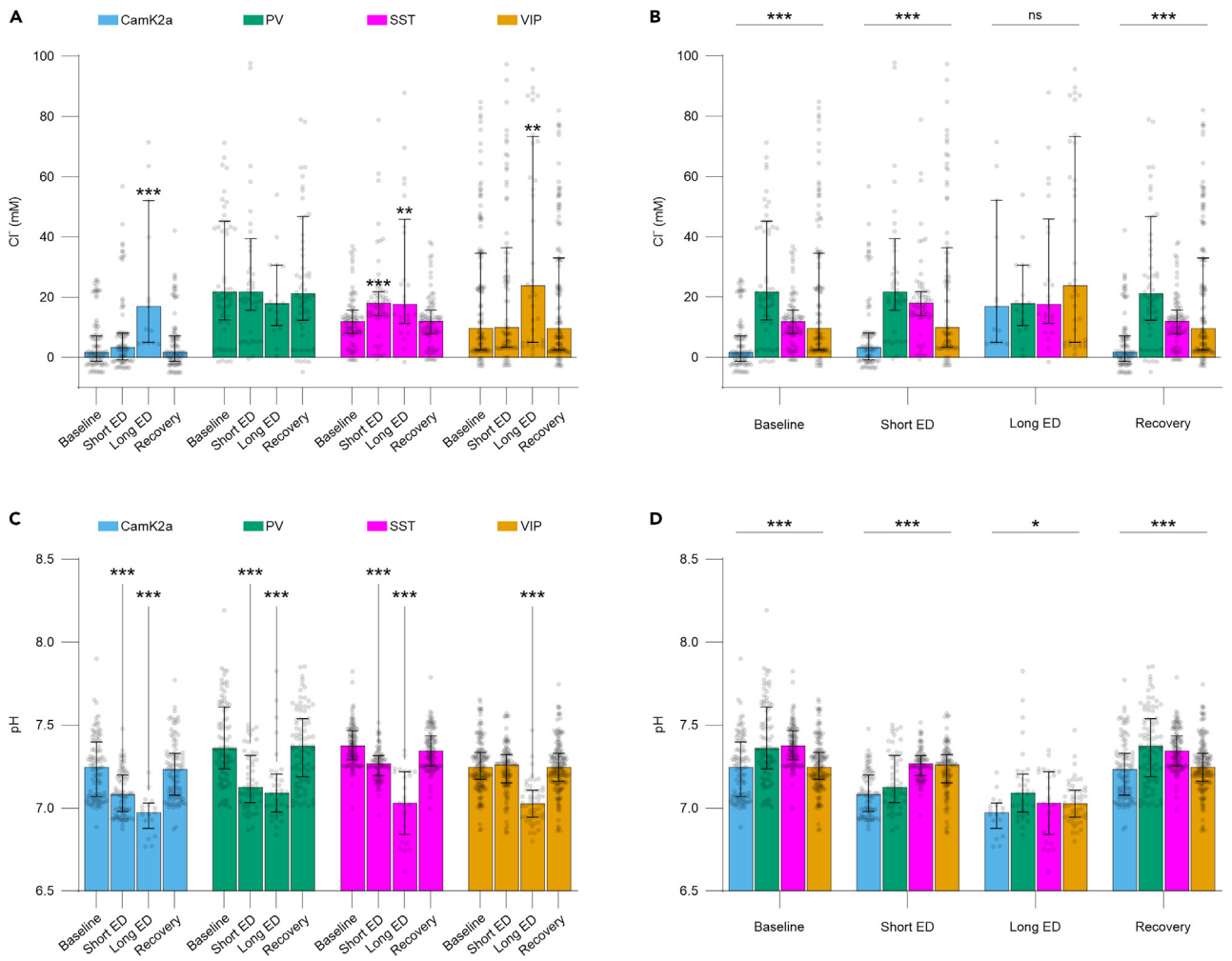

Figure 7. Neuronal subtypes exhibit converging intracellular chloride concentrations and acidify during an ED

(A) Subtypes differed in their chloride changes during an ED. EDs were divided into short EDs (less than 60s) and long EDs (greater than 60s), and compared to baseline levels before the ED and recovery levels after the ED. PV interneurons were the only subtype that did not exhibit a change in chloride (PV $\chi^2_{(3)} = 1.28$, $p = 0.7335$, Kruskal-Wallis test). CamK2a neurons, SST interneurons, and VIP interneurons each exhibited a significant change in chloride during an ED (CamK2a $\chi^2_{(3)} = 19.89$, $p < 0.0002$; SST $\chi^2_{(3)} = 31.75$, $p < 0.0001$; VIP $\chi^2_{(3)} = 13.33$, $p < 0.004$). Y axis is limited to 100 mM for plotting purposes. Bars and lines indicate median and IQR, dots indicate individual EDs. Asterisks indicate p values from post-hoc Dunn's multiple comparisons tests comparing to baseline within each subtype. N = 93 EDs from 23 CamK2a neurons in 15 slices, 60 EDs from 28 PV interneurons in 26 slices, 88 EDs from 32 SST interneurons in 12 slices, 123 EDs from 44 VIP interneurons in 26 slices.

(B) Subtype chloride levels converged during an ED. Chloride levels differed across the neuronal subtypes under baseline conditions (Baseline $\chi^2_{(3)} = 76.92$, $p < 0.0001$, Kruskal-Wallis test) and during short EDs (Short ED $\chi^2_{(3)} = 51.21$, $p < 0.0001$), but became indistinguishable during long EDs (Long ED $\chi^2_{(3)} = 1.46$, $p = 0.6918$). Subtype differences were re-established after the EDs (Recovery $\chi^2_{(3)} = 74.65$, $p < 0.0001$). Data replotted from "A" using same conventions. Asterisks indicate p values from Kruskal-Wallis tests comparing across subtypes.

(C) All subtypes acidified during and ED, typically showing acidic shifts during even short EDs (CamK2a $\chi^2_{(3)} = 60.74$, $p < 0.0001$, Kruskal-Wallis test; PV $\chi^2_{(3)} = 57.58$, $p < 0.0001$; SST $\chi^2_{(3)} = 93.53$, $p < 0.0001$; VIP $\chi^2_{(3)} = 76.57$, $p < 0.0001$). Bars and lines indicate median and IQR, dots indicate individual EDs. Asterisks indicate p values from post-hoc Dunn's multiple comparisons tests comparing to baseline within each subtype.

(D) While all subtypes acidified during an ED, they exhibited differences in absolute pH (Baseline $\chi^2_{(3)} = 62.55$, $p < 0.0001$, Kruskal-Wallis test; Short ED $\chi^2_{(3)} = 65.45$, $p < 0.0001$; Long ED $\chi^2_{(3)} = 8.286$, $p = 0.041$; Recovery $\chi^2_{(3)} = 49.97$, $p < 0.0001$). Data replotted from "C" using same conventions. Asterisks indicate p values from Kruskal-Wallis tests comparing across subtypes. * indicates $p < 0.05$, ** indicates $p < 0.01$, *** indicates $p < 0.001$.

neuronal subtypes (Figure 6). In this analysis, we normalized for ED duration so that 0% indicated the start of the ED and 100% indicated the end of the ED, as defined by the membrane potential (Vm) dynamics recorded from a nearby pyramidal neuron. This revealed that while the time course of the ED's network activity was comparable across the four subtypes (Vm; Figures 6A–6D), there were consistent differences in chloride and pH dynamics.

In terms of chloride dynamics, CamK2a pyramidal neurons exhibited significant increases in their intracellular chloride during EDs, which peaked toward the end of the ED (Figure 6A), consistent with previous electrophysiological and imaging data.[6,9,10,27,28,45] To capture this, we extracted each neuron's peak ED-associated chloride level, relative to the baseline before ED onset. Across the population, an ED was associated with a significant transient increase in chloride in CamK2a neurons (median 1.9 mM, IQR [1.2 to 7.2 mM]; $p < 0.0001$, compared to zero, Wilcoxon signed-rank test). Similar to pyramidal neurons, an ED caused a transient increase in the chloride levels of SST interneurons (7.9 mM, IQR [1.3 to 12.5 mM]; $p < 0.0001$) and VIP interneurons (2.3 mM, IQR [0.7 to 10.4 mM]; $p < 0.0001$), which peaked toward the end of the ED (Figures 6C and 6D). However, in contrast to the other subtypes, chloride fluxes in PV interneurons were much more modest, such that there was no net change in chloride (Figure 6B; −2.60 mM, IQR [−16.7 to 4.1 mM]; $p = 0.09$, Wilcoxon signed-rank test). Statistical comparisons between the subtypes supported these observations. CamK2a neurons, SST interneurons, and VIP interneurons all exhibited a greater change in intracellular chloride than PV interneurons ($\chi^2_{(3)} = 28.75$, $p < 0.0001$, Kruskal-Wallis test, followed by post-hoc Dunn's multiple comparisons tests; CamK2a vs PV, $p = 0.0014$; CamK2a vs SST, $p = 0.3479$; CamK2a vs VIP, $p > 0.9999$; PV vs SST, $p < 0.0001$; PV vs VIP, $p = 0.001$; SST vs VIP, $p = 0.1905$).

All subtypes exhibited acidic transients during an ED, which started with the onset of the ED and typically lasted beyond the end of the ED (Figures 6A–6D). This observation was confirmed when we extracted each neuron's peak ED-associated pH change, relative to the value before ED onset (CamK2a median −0.14, IQR [−0.27 to −0.08]; PV median −0.25 [−0.39 to −0.13]; SST median −0.14 [−0.21 to −0.03]; VIP median −0.10 [−0.11 to −0.01]; $p < 0.0001$ compared to zero in each case, Wilcoxon signed-rank test). Comparisons between the subtypes revealed that EDs generated acidic pH shifts of similar amplitude in pyramidal neurons and SST interneurons, while PV interneurons showed the largest acidic shift and VIP interneurons the smallest acidic shift ($\chi^2_{(3)} = 86.74$, $p < 0.0001$, Kruskal-Wallis test, followed by post-hoc Dunn's multiple comparisons tests; CamK2a vs PV, $p = 0.0351$; CamK2a vs SST, $p > 0.9999$; CamK2a vs VIP, $p < 0.0001$; PV vs SST, $p = 0.0002$; PV vs VIP, $p < 0.0001$; SST vs VIP, $p < 0.0001$).

In the final analysis we examined the impact of the duration of the ED (Figure 7). EDs with a duration shorter than 60 s were classified as "short EDs" (mean duration of 24.7 $\pm$ 0.7 s) and EDs lasting longer than 60 s were classified as "long EDs" (mean duration of 199.6 $\pm$ 12.6 s). Interestingly, while chloride increases were evident in SST interneurons for both short and long EDs, the increases in CamK2a pyramidal neurons and VIP interneurons became evident following long EDs (Figure 7A). PV interneurons were unique, in the sense that their chloride remained stable throughout epileptiform activity and exhibited no detectable change during either short or long EDs (Figure 7A). Furthermore, this analysis revealed that during periods of intense epileptiform activity, the different neuronal subtypes tended to converge on a common intracellular chloride concentration of approximately 20 mM. In other words, the differences in subtype chloride at baseline ($p < 0.0001$, $\chi^2_{(3)} = 76.92$, Kruskal-Wallis test), were no longer present during long EDs ($p = 0.6918$, $\chi^2_{(3)} = 1.46$, Kruskal-Wallis test; Figure 7B).

Finally, in terms of pH changes as a function of the duration of the epileptiform activity, acidification was already evident for short EDs in CamK2a pyramidal neurons, PV interneurons, and SST interneurons (Figure 7C). Long EDs resulted in acidification in all subtypes ($p < 0.0001$ for each subtype, Kruskal-Wallis test), small differences between the subtypes in their absolute pH levels were evident across the epileptiform activity, and all neurons recovered to baseline values once the ED had ended, consistent with the acidification being a transient effect (Figure 7D).

DISCUSSION

Here we present a Cre-dependent version of ClopHensorN—a genetically encoded ratiometric reporter of chloride and pH, which is optimized for the nervous system. This new tool allowed us to determine the activity-related dynamics of intracellular chloride and pH in genetically defined neuronal subtypes of the mouse hippocampus during *in vitro* epileptiform activity. Simultaneous chloride and pH imaging was performed in CamK2a pyramidal neurons, as well as in PV, SST, and VIP interneurons. Imaging of the floxed ClopHensorN revealed that neuronal subtypes exhibit different baseline intracellular chloride levels with PV interneurons exhibiting the highest somatic chloride. During an ED, however, these neuronal subtypes converge upon a common, high intracellular chloride level. Floxed ClopHensorN imaging revealed that the neuronal subtypes also acidified to different degrees during an ED, underscoring the importance of the

reporter's ability to dissociate chloride and proton fluxes, compared to alternative reporters that confound these ion species. The ability to dissociate these two ions in a way that relates to the intensity of epileptiform activity may have diagnostic implications. Changes in somatic pH could be considered a more sensitive readout of shorter-duration ED activity, while changes in somatic chloride could be considered a readout of more sustained epileptiform activity.

Consistent with previous electrophysiological evidence that E_{GABA_A} is relatively depolarized in interneurons,[15–17,20–22] we found that GABAergic interneurons tend to exhibit higher baseline somatic chloride levels than pyramidal neurons. This is best exemplified by PV interneurons, which exhibited the highest baseline somatic chloride levels of approximately 20 mM. Based on the Nernst equation, this would predict a chloride reversal potential of approximately −50 mV, which is comparable to estimates of E_{GABA_A} from gramicidin perforated patch recordings in fast-spiking interneurons and PV interneurons,[18,21] although there are also likely to be effects of age.[20,22] Such neuronal subtype differences in intracellular chloride presumably reflect the differential contribution of chloride regulatory mechanisms such as cation-chloride co-transporters,[18,20,51] other transporters such as Na^+/Cl^- co-transporters and Cl^-/HCO_3^- exchangers,[52] impermeant anions,[53,54] and chloride-permeable ion channels such as ligand-gated $GABA_A$Rs.[55] Future work could investigate the molecular mechanisms and functional significance of chloride regulation in the different neuronal subtypes. In the case of interneurons, their relatively high baseline somatic chloride may be integral to their function within the network. For example, PV interneurons have been reported to use shunting inhibition rather than hyperpolarizing inhibition to promote coherent oscillatory activity in interneuron networks.[21] Chloride levels can also influence a neuron's excitability via Ca^{2+}-dependent chloride channels, which couple excitatory post-synaptic potentials and action potential generation.[56,57]

We confirmed previous observations that pyramidal neurons exhibit a pronounced but transient accumulation in intracellular chloride during an ED.[6,9,27,28,58] Taking advantage of our floxed ClopHensorN reporter, we were also able to compare the three main populations of GABAergic interneurons under the same conditions. Like pyramidal neurons, SST and VIP interneurons tended to accumulate chloride during EDs. This was in contrast to the PV interneuron population, whose intracellular chloride levels remained unchanged during epileptifom activity. These differences are unlikely to reflect ED-associated damage, as the neuronal populations recovered their ion concentrations following each ED. Rather, the degree of loading across the subtypes appeared to be inversely related to the baseline chloride levels, suggesting that the initial driving force of the $GABA_A$R influences the degree of ED-associated chloride shift. This is consistent with the observation that with intense periods of epileptiform activity, all neuronal subtypes converged toward a common, high intracellular chloride level of approximately 20 mM. Such a concentration would predict that the chloride reversal potential in all subtypes would also converge toward a value of approximately −50 mV, which is consistent with electrophysiological estimates of how E_{GABA_A} changes in pyramidal neurons during an ED.[10,58] Our chloride imaging data, therefore, suggest that GABAergic synaptic inputs to the different neuronal subtypes will exhibit different chloride-dependent changes during an ED. For example, while pyramidal neurons experience a chloride load that switches their GABAergic inputs from being hyperpolarizing to depolarizing and even excitatory during an ED,[6,10,58] the chloride levels suggest that the effect of GABAergic synaptic transmission onto PV interneurons remains more stable throughout an ED. Interestingly, shorter EDs led to detectable chloride increases in SST interneurons, but not in pyramidal neurons or VIP interneurons. This supports the general idea that the intensity of the epileptiform activity determines the degree of chloride change, and suggests that more prolonged EDs are required to elicit detectable changes in somatic chloride. Our data does not exclude the possibility that shorter EDs impose intracellular chloride changes within other cellular compartments, such as the neurons' processes. Given that ClopHensorN is expressed throughout the cytoplasm, an interesting direction for future work would be to investigate chloride dynamics within the dendrites and axons of the different neuronal subtypes.

In terms of intracellular pH levels, our baseline measurements revealed modest but statistically significant differences between the neuronal subtypes, and that all subtypes exhibited acidic shifts during an ED, although the size of the acidic shift differed. While our estimates of baseline and dynamic pH in pyramidal neurons were consistent with previous studies,[46–48] we are not aware of any previous reports regarding intracellular pH in subtypes of GABAergic interneurons. Among the interneuron populations, VIP interneurons exhibited the lowest baseline intracellular pH and the smallest acidic shift during an ED. It is interesting to contrast this population with the PV interneurons, which exhibited the most alkaline baseline

pH and the largest acidic shifts during an ED. Population differences could reflect the relative contribution of transporter proteins or neuron-specific differences in buffering capacity, which may be affected by gap junction coupling within the populations.[59,60] It will therefore be interesting to examine candidate mechanisms in the future, ideally by using manipulations that can also be targeted to the specific neuronal population of interest. In terms of the ED-related changes in pH, multiple mechanisms link periods of elevated neural activity to intracellular acidification, including the metabolic production of acid equivalents such as CO_2 and lactic acid,[61,62] the release of protons from intracellular stores triggered by increased cytoplasmic Ca^{2+},[63] the influx of protons via plasmalemmal Ca^{2+}-ATPases,[64,65] or the entry of acid equivalents through voltage-gated or ligand-gated channels, including HCO_3^- efflux through $GABA_A$ receptors.[1,66] The more pronounced acidification of PV interneurons during epileptiform activity may therefore reflect the particularly high firing rates of this interneuron subtype, which may cause faster production of acid equivalents, for example.

Meanwhile, the differences in baseline pH may reflect trade-offs between excitability and neuroprotective mechanisms. Lower intracellular pH is associated with lower levels of cytosolic Ca^{2+} and the suppression of membrane conductances associated with neuronal excitability.[67–70] The lower baseline cytosolic pH of VIP interneurons could, therefore, reflect a neuroprotective state in this interneuron type, which limits excitability and potential excitotoxic effects associated with Ca^{2+} mobilization.[70,71] Whereas the higher baseline pH of PV interneurons could reflect the highly excitable state of this neuronal population, which is primed to respond rapidly to network activity and may have evolved alternative strategies to mitigate the associated risks and energetic demands.[72]

In summary, we develop and utilize a Cre-dependent, ratiometric, and simultaneous reporter of chloride and pH, in order to compare genetically defined neuronal subtypes. Our data from mouse hippocampus reveal that the major excitatory and inhibitory neuronal populations differ substantially in their baseline concentrations and the dynamics that they exhibit during epileptiform activity. We make our Cre-dependent ClopHensorN available to the scientific community and imagine that this tool will be useful in investigating genetically defined cell types across a variety of brain regions and conditions. Future work could also combine this tool with cell-targeted manipulations to investigate the mechanisms that underlie cell-specific differences in ion regulation.

Limitations of the study

While our genetic targeting of ClopHensorN provides the first comparison of neuron-specific pH and chloride dynamics during epileptiform activity, it is worth highlighting some limitations. Firstly, there are a number of technical considerations with using this ratiometric fluorescent reporter. This includes the fact that each imaging system requires calibration so that the optical signals can be translated into absolute ion concentrations. This process uses averaged measurements from cell populations whose ion concentrations are experimentally clamped, meaning that calibration is sensitive to the efficacy of the ionic clamping. In the case of ClopHensor, the use of multiple wavelengths can pose a further challenge due to the differential absorption and scattering effects of brain tissue.[28] This effect is modest when imaging neurons close to the surface of a brain slice, but is more pronounced at greater tissue depths, such as when using multiphoton imaging *in vivo*. It has been shown that this effect can be quantified and then corrected through control experiments.[28] Alternatively, the use of fiber photometry to image directly in the brain could simplify the optics and afford opportunities to monitor ion dynamics in freely behaving animals. Meanwhile, one feature of the genetic targeting strategy is that the data for each neuronal population are derived across different brain slices and mice, rather than simultaneously from the different neuronal populations as they experience the same network activity. And finally, it is worth considering the fact that our study has used mouse organotypic hippocampal brain slices to reveal the distinct basal and activity-dependent ion dynamics in genetically defined neuronal subtypes. This experimental system represents a reliable model of epileptiform activity and provides good optical access and the opportunity to combine imaging and simultaneous electrophysiological recordings. It is nevertheless an *in vitro* model system, which is not equivalent to the awake, intact brain, and therefore only affords the chance to study seizure-like activity. Neurons in organotypic hippocampal slices maintain many of the morphological and signaling characteristics of age-matched neurons in the intact hippocampus.[37,45] However, the tissue suffers a loss of afferent connections from other brain structures, which is believed to lead to axonal sprouting and the generation of recurrent excitatory connections.[73] This may recapitulate aspects of temporal lobe epilepsy,[74–77] but it would be interesting to quantify these neuron-specific ion dynamics in other models of epilepsy.

STAR★METHODS

Detailed methods are provided in the online version of this paper and include the following:

- KEY RESOURCES TABLE
- RESOURCE AVAILABILITY
  - Lead contact
  - Materials availability
  - Data and code availability
- EXPERIMENTAL MODEL AND SUBJECT DETAILS
  - Preparation of organotypic hippocampal brain slices
- METHOD DETAILS
  - Generating the floxed ClopHensorN construct
  - Viral transduction of brain slices
  - Electrophysiological recordings and epileptiform activity
  - ClopHensorN imaging of intracellular chloride and pH
  - ClopHensorN calibration
- QUANTIFICATION AND STATISTICAL ANALYSIS

ACKNOWLEDGMENTS

We would like to thank members of the Akerman lab for advice and comments. The research leading to these results has received funding from the European Research Council under grant agreement 617670, and MRC project MR/S01134X/1. In addition, A.C. was supported by a Wellcome Trust Doctoral Fellowship [102364/Z/13/Z] and T.W. by a Royal Society Newton International Fellowship. J.V.R. was supported by the National Research Foundation of South Africa, a Wellcome Trust Seed Award (214042/Z/18/Z), the South African Medical Research Council and by the FLAIR Fellowship Program (FLR\R1\190829): a partnership between the African Academy of Sciences and the Royal Society funded by the UK Government's Global Challenges Research Fund. S.E.N. was supported by a Royal Society Dorothy Hodgkin Fellowship.

AUTHOR CONTRIBUTIONS

A.C. and C.J.A. conceived the project and designed the experiments. A.C. and T.W. performed the experiments, J.V.R advised on the imaging methodology and data analysis, T.W. and S.E.N. generated the molecular tools, A.C. analyzed the data and prepared the figures. A.C. and C.J.A. wrote the manuscript with input from all authors.

DECLARATION OF INTERESTS

The authors declare no competing interests. The manuscript was approved by all of the authors.

INCLUSION AND DIVERSITY

We support inclusive, diverse, and equitable conduct of research.

Received: November 20, 2022
Revised: February 3, 2023
Accepted: March 5, 2023
Published: March 9, 2023

REFERENCES

1. Kaila, K., and Voipio, J. (1987). Postsynaptic fall in intracellular pH induced by GABA-activated bicarbonate conductance. Nature *330*, 163–165. https://doi.org/10.1038/330163a0.

2. Kaila, K., Pasternack, M., Saarikoski, J., and Voipio, J. (1989). Influence of GABA-gated bicarbonate conductance on potential, current and intracellular chloride in crayfish muscle fibres. J. Physiol. *416*, 161–181.

3. Thompson, S.M., and Gähwiler, B.H. (1989). Activity-dependent disinhibition. I. Repetitive stimulation reduces IPSP driving force and conductance in the hippocampus in vitro. J. Neurophysiol. *61*, 501–511. https://doi.org/10.1152/jn.1989.61.3.501.

4. Staley, K.J., Soldo, B.L., and Proctor, W.R. (1995). Ionic mechanisms of neuronal excitation by inhibitory GABAA receptors. Science *269*, 977–981.

5. Staley, K.J., and Proctor, W.R. (1999). Modulation of mammalian dendritic GABA(A) receptor function by the kinetics of Cl- and HCO3- transport. J. Physiol. *519*, 693–712.

6. Isomura, Y., Sugimoto, M., Fujiwara-Tsukamoto, Y., Yamamoto-Muraki, S., Yamada, J., and Fukuda, A. (2003). Synaptically activated Cl- accumulation responsible for depolarizing GABAergic

responses in mature hippocampal neurons. J. Neurophysiol. *90*, 2752–2756. https://doi.org/10.1152/jn.00142.2003.

7. Fujiwara-Tsukamoto, Y., Isomura, Y., and Takada, M. (2006). Comparable GABAergic mechanisms of hippocampal seizurelike activity in posttetanic and low-Mg2+ conditions. J. Neurophysiol. *95*, 2013–2019. https://doi.org/10.1152/jn.00238.2005.

8. Fujiwara-Tsukamoto, Y., Isomura, Y., Imanishi, M., Fukai, T., and Takada, M. (2007). Distinct types of ionic modulation of GABA actions in pyramidal cells and interneurons during electrical induction of hippocampal seizure-like network activity. Eur. J. Neurosci. *25*, 2713–2725. https://doi.org/10.1111/j.1460-9568.2007.05543.x.

9. Lillis, K.P., Kramer, M.A., Mertz, J., Staley, K.J., and White, J.A. (2012). Pyramidal cells accumulate chloride at seizure onset. Neurobiol. Dis. *47*, 358–366. https://doi.org/10.1016/j.nbd.2012.05.016.

10. Ellender, T.J., Raimondo, J.V., Irkle, A., Lamsa, K.P., and Akerman, C.J. (2014). Excitatory effects of parvalbumin-expressing interneurons maintain hippocampal epileptiform activity via synchronous afterdischarges. J. Neurosci. *34*, 15208–15222. https://doi.org/10.1523/JNEUROSCI.1747-14.2014.

11. Köhling, R., Vreugdenhil, M., Bracci, E., and Jefferys, J.G. (2000). Ictal epileptiform activity is facilitated by hippocampal GABAA receptor-mediated oscillations. J. Neurosci. *20*, 6820–6829. https://doi.org/10.1523/JNEUROSCI.20-18-06820.2000.

12. D'Antuono, M., Louvel, J., Köhling, R., Mattia, D., Bernasconi, A., Olivier, A., Turak, B., Devaux, A., Pumain, R., and Avoli, M. (2004). GABAA receptor-dependent synchronization leads to ictogenesis in the human dysplastic cortex. Brain *127*, 1626–1640. https://doi.org/10.1093/brain/awh181.

13. Fujiwara-Tsukamoto, Y., Isomura, Y., Imanishi, M., Ninomiya, T., Tsukada, M., Yanagawa, Y., Fukai, T., and Takada, M. (2010). Prototypic seizure activity driven by mature hippocampal fast-spiking interneurons. J. Neurosci. *30*, 13679–13689. https://doi.org/10.1523/JNEUROSCI.1523-10.2010.

14. Magloire, V., Cornford, J., Lieb, A., Kullmann, D.M., and Pavlov, I. (2019). KCC2 overexpression prevents the paradoxical seizure-promoting action of somatic inhibition. Nat. Commun. *10*, 1225. https://doi.org/10.1038/s41467-019-08933-4.

15. Banke, T.G., and McBain, C.J. (2006). GABAergic input onto CA3 hippocampal interneurons remains shunting throughout development. J. Neurosci. *26*, 11720–11725. https://doi.org/10.1523/JNEUROSCI.2887-06.2006.

16. Golding, N.L., and Oertel, D. (1996). Context-dependent synaptic action of glycinergic and GABAergic inputs in the dorsal cochlear nucleus. J. Neurosci. *16*, 2208–2219. https://doi.org/10.1523/JNEUROSCI.16-07-02208.1996.

17. Chavas, J., and Marty, A. (2003). Coexistence of excitatory and inhibitory GABA synapses in the cerebellar interneuron network. J. Neurosci. *23*, 2019–2031.

18. Martina, M., Royer, S., and Paré, D. (2001). Cell-type-specific GABA responses and chloride homeostasis in the cortex and amygdala. J. Neurophysiol. *86*, 2887–2895. https://doi.org/10.1152/jn.2001.86.6.2887.

19. Verheugen, J.A., Fricker, D., and Miles, R. (1999). Noninvasive measurements of the membrane potential and GABAergic action in hippocampal interneurons. J. Neurosci. *19*, 2546–2555. https://doi.org/10.1523/JNEUROSCI.19-07-02546.1999.

20. Otsu, Y., Donneger, F., Schwartz, E.J., and Poncer, J.C. (2020). Cation-chloride cotransporters and the polarity of GABA signalling in mouse hippocampal parvalbumin interneurons. J. Physiol. *598*, 1865–1880. https://doi.org/10.1113/JP279221.

21. Vida, I., Bartos, M., and Jonas, P. (2006). Shunting inhibition improves robustness of gamma oscillations in hippocampal interneuron networks by homogenizing firing rates. Neuron *49*, 107–117. https://doi.org/10.1016/j.neuron.2005.11.036.

22. Sauer, J.-F., and Bartos, M. (2010). Recruitment of early postnatal parvalbumin-positive hippocampal interneurons by GABAergic excitation. J. Neurosci. *30*, 110–115. https://doi.org/10.1523/JNEUROSCI.4125-09.2010.

23. Patenaude, C., Massicotte, G., and Lacaille, J.-C. (2005). Cell-type specific GABA synaptic transmission and activity-dependent plasticity in rat hippocampal stratum radiatum interneurons. Eur. J. Neurosci. *22*, 179–188. https://doi.org/10.1111/j.1460-9568.2005.04207.x.

24. Kuner, T., and Augustine, G.J. (2000). A genetically encoded ratiometric indicator for chloride: capturing chloride transients in cultured hippocampal neurons. Neuron *27*, 447–459. https://doi.org/10.1016/S0896-6273(00)00056-8.

25. Markova, O., Mukhtarov, M., Real, E., Jacob, Y., and Bregestovski, P. (2008). Genetically encoded chloride indicator with improved sensitivity. J. Neurosci. Methods *170*, 67–76. https://doi.org/10.1016/j.jneumeth.2007.12.016.

26. Arosio, D., Ricci, F., Marchetti, L., Gualdani, R., Albertazzi, L., and Beltram, F. (2010). Simultaneous intracellular chloride and pH measurements using a GFP-based sensor. Nat. Methods *7*, 516–518. https://doi.org/10.1038/nmeth.1471.

27. Raimondo, J.V., Joyce, B., Kay, L., Schlagheck, T., Newey, S.E., Srinivas, S., and Akerman, C.J. (2013). A genetically-encoded chloride and pH sensor for dissociating ion dynamics in the nervous system. Front. Cell. Neurosci. *7*, 202. https://doi.org/10.3389/fncel.2013.00202.

28. Sulis Sato, S., Artoni, P., Landi, S., Cozzolino, O., Parra, R., Pracucci, E., Trovato, F., Szczurkowska, J., Luin, S., Arosio, D., et al. (2017). Simultaneous two-photon imaging of intracellular chloride concentration and pH in mouse pyramidal neurons in vivo. Proc. Natl. Acad. Sci. USA *114*, E8770–E8779. https://doi.org/10.1073/pnas.1702861114.

29. Heinemann, U., and Lux, H.D. (1977). Ceiling of stimulus induced rises in extracellular potassium concentration in the cerebral cortex of cat. Brain Res. *120*, 231–249. https://doi.org/10.1016/0006-8993(77)90903-9.

30. Dreier, J.P., and Heinemann, U. (1991). Regional and time dependent variations of low Mg2+ induced epileptiform activity in rat temporal cortex slices. Exp. Brain Res. *87*, 581–596. https://doi.org/10.1007/BF00227083.

31. Kaila, K., Lamsa, K., Smirnov, S., Taira, T., and Voipio, J. (1997). Long-lasting GABA-mediated depolarization evoked by high-frequency stimulation in pyramidal neurons of rat hippocampal slice is attributable to a network-driven, bicarbonate-dependent K+ transient. J. Neurosci. *17*, 7662–7672.

32. Xiong, Z.-Q., Saggau, P., and Stringer, J.L. (2000). Activity-dependent intracellular acidification correlates with the duration of seizure activity. J. Neurosci. *20*, 1290–1296. https://doi.org/10.1523/JNEUROSCI.20-04-01290.2000.

33. Dyhrfjeld-Johnsen, J., Berdichevsky, Y., Swiercz, W., Sabolek, H., and Staley, K.J. (2010). Interictal spikes precede ictal discharges in an organotypic hippocampal slice culture model of epileptogenesis. J. Clin. Neurophysiol. *27*, 418–424. https://doi.org/10.1097/WNP.0b013e3181fe0709.

34. Călin, A., Stancu, M., Zagrean, A.-M., Jefferys, J.G.R., Ilie, A.S., and Akerman, C.J. (2018). Chemogenetic recruitment of specific interneurons suppresses seizure activity. Front. Cell. Neurosci. *12*, 293. https://doi.org/10.3389/fncel.2018.00293.

35. Berdichevsky, Y., Dzhala, V., Mail, M., and Staley, K.J. (2012). Interictal spikes, seizures and ictal cell death are not necessary for post-traumatic epileptogenesis in vitro. Neurobiol. Dis. *45*, 774–785. https://doi.org/10.1016/j.nbd.2011.11.001.

36. Streit, P., Thompson, S.M., and Gähwiler, B.H. (1989). Anatomical and physiological properties of GABAergic neurotransmission in organotypic slice cultures of rat Hippocampus. Eur. J. Neurosci. *1*, 603–615. https://doi.org/10.1111/j.1460-9568.1989.tb00366.x.

37. De Simoni, A., Griesinger, C.B., and Edwards, F.A. (2003). Development of rat CA1 neurones in acute versus organotypic slices: role of experience in synaptic morphology and activity. J. Physiol. *550*, 135–147. https://doi.org/10.1113/jphysiol.2003.039099.

38. Di Cristo, G., Wu, C., Chattopadhyaya, B., Ango, F., Knott, G., Welker, E., Svoboda, K., and Huang, Z.J. (2004). Subcellular domain-restricted GABAergic innervation in primary visual cortex in the absence of sensory and

thalamic inputs. Nat. Neurosci. *7*, 1184–1186. https://doi.org/10.1038/nn1334.

39. Pawelzik, H., Hughes, D.I., and Thomson, A.M. (2002). Physiological and morphological diversity of immunocytochemically defined parvalbumin- and cholecystokinin-positive interneurones in CA1 of the adult rat hippocampus. J. Comp. Neurol. *443*, 346–367. https://doi.org/10.1002/cne.10118.

40. Bartos, M., and Elgueta, C. (2012). Functional characteristics of parvalbumin- and cholecystokinin-expressing basket cells. J. Physiol. *590*, 669–681. https://doi.org/10.1113/jphysiol.2011.226175.

41. Köhler, C. (1982). Distribution and morphology of vasoactive intestinal polypeptide-like immunoreactive neurons in regio superior of the rat hippocampal formation. Neurosci. Lett. *33*, 265–270. https://doi.org/10.1016/0304-3940(82)90382-2.

42. Taniguchi, H., He, M., Wu, P., Kim, S., Paik, R., Sugino, K., Kvitsiani, D., Fu, Y., Lu, J., Lin, Y., et al. (2011). A resource of cre driver lines for genetic targeting of GABAergic neurons in cerebral cortex. Neuron *71*, 995–1013. https://doi.org/10.1016/j.neuron.2011.07.026.

43. Boyarsky, G., Ganz, M.B., Sterzel, R.B., and Boron, W.F. (1988). pH regulation in single glomerular mesangial cells. I. Acid extrusion in absence and presence of HCO3-. Am. J. Physiol. *255*, C844–C856. https://doi.org/10.1152/ajpcell.1988.255.6.C844.

44. Grynkiewicz, G., Poenie, M., and Tsien, R.Y. (1985). A new generation of Ca2+ indicators with greatly improved fluorescence properties. J. Biol. Chem. *260*, 3440–3450.

45. Ilie, A., Raimondo, J.V., and Akerman, C.J. (2012). Adenosine release during seizures attenuates GABAA receptor-mediated depolarization. J. Neurosci. *32*, 5321–5332. https://doi.org/10.1523/JNEUROSCI.5412-11.2012.

46. Raimondo, J.V., Irkle, A., Wefelmeyer, W., Newey, S.E., and Akerman, C.J. (2012). Genetically encoded proton sensors reveal activity-dependent pH changes in neurons. Front. Mol. Neurosci. *5*, 68. https://doi.org/10.3389/fnmol.2012.00068.

47. Caspers, H., and Speckmann, E.-J. (1972). Cerebral pO2, pCO2 and pH: changes during convulsive activity and their significance for spontaneous arrest of seizures. Epilepsia *13*, 699–725. https://doi.org/10.1111/j.1528-1157.1972.tb04403.x.

48. Raimondo, J.V., Burman, R.J., Katz, A.A., and Akerman, C.J. (2015). Ion dynamics during seizures. Front. Cell. Neurosci. *9*, 419. https://doi.org/10.3389/fncel.2015.00419.

49. Lillis, K.P., Wang, Z., Mail, M., Zhao, G.Q., Berdichevsky, Y., Bacskai, B., and Staley, K.J. (2015). Evolution of network synchronization during early epileptogenesis parallels synaptic circuit alterations. J. Neurosci. *35*, 9920–9934. https://doi.org/10.1523/JNEUROSCI.4007-14.2015.

50. Călin, A., Ilie, A.S., and Akerman, C.J. (2021). Disrupting epileptiform activity by preventing parvalbumin interneuron depolarization block. J. Neurosci. *41*, 9452–9465. https://doi.org/10.1523/JNEUROSCI.1002-20.2021.

51. Rivera, C., Voipio, J., Payne, J.A., Ruusuvuori, E., Lahtinen, H., Lamsa, K., Pirvola, U., Saarma, M., and Kaila, K. (1999). The K+/Cl- co-transporter KCC2 renders GABA hyperpolarizing during neuronal maturation. Nature *397*, 251–255. https://doi.org/10.1038/16697.

52. Doyon, N., Vinay, L., Prescott, S.A., and De Koninck, Y. (2016). Chloride regulation: a dynamic equilibrium crucial for synaptic inhibition. Neuron *89*, 1157–1172. https://doi.org/10.1016/j.neuron.2016.02.030.

53. Glykys, J., Dzhala, V., Egawa, K., Balena, T., Saponjian, Y., Kuchibhotla, K.V., Bacskai, B.J., Kahle, K.T., Zeuthen, T., and Staley, K.J. (2014). Local impermeant anions establish the neuronal chloride concentration. Science *343*, 670–675. https://doi.org/10.1126/science.1245423.

54. Düsterwald, K.M., Currin, C.B., Burman, R.J., Akerman, C.J., Kay, A.R., and Raimondo, J.V. (2018). Biophysical models reveal the relative importance of transporter proteins and impermeant anions in chloride homeostasis. Elife *7*, e39575. https://doi.org/10.7554/eLife.39575.

55. Jentsch, T.J., Stein, V., Weinreich, F., and Zdebik, A.A. (2002). Molecular structure and physiological function of chloride channels. Physiol. Rev. *82*, 503–568. https://doi.org/10.1152/physrev.00029.2001.

56. Huang, W.C., Xiao, S., Huang, F., Harfe, B.D., Jan, Y.N., and Jan, L.Y. (2012). Calcium-Activated chloride channels (CaCCs) regulate action potential and synaptic response in hippocampal neurons. Neuron *74*, 179–192. https://doi.org/10.1016/j.neuron.2012.01.033.

57. Sørensen, A.T., Ledri, M., Melis, M., Nikitidou Ledri, L., Andersson, M., and Kokaia, M. (2017). Altered chloride homeostasis decreases the action potential threshold and increases hyperexcitability in hippocampal neurons. eNeuro *4*. https://doi.org/10.1523/ENEURO.0172-17.2017.

58. Burman, R.J., Selfe, J.S., Lee, J.H., van den Berg, M., Călin, A., Codadu, N.K., Wright, R., Newey, S.E., Parrish, R.R., Katz, A.A., et al. (2019). Excitatory GABAergic signalling is associated with benzodiazepine resistance in status epilepticus. Brain *142*, 3482–3501. https://doi.org/10.1093/brain/awz283.

59. Fukuda, T., and Kosaka, T. (2000). Gap junctions linking the dendritic network of GABAergic interneurons in the Hippocampus. J. Neurosci. *20*, 1519–1528. https://doi.org/10.1523/JNEUROSCI.20-04-01519.2000.

60. Traub, R.D., Kopell, N., Bibbig, A., Buhl, E.H., LeBeau, F.E., and Whittington, M.A. (2001). Gap junctions between interneuron dendrites can enhance synchrony of gamma oscillations in distributed networks. J. Neurosci. *21*, 9478–9486. https://doi.org/10.1523/JNEUROSCI.21-23-09478.2001.

61. Siesjö, B.K. (1985). Acid-base homeostasis in the brain: physiology, chemistry, and neurochemical pathology. Prog. Brain Res. *63*, 121–154. https://doi.org/10.1016/S0079-6123(08)61980-9.

62. Zhan, R.Z., Fujiwara, N., Tanaka, E., and Shimoji, K. (1998). Intracellular acidification induced by membrane depolarization in rat hippocampal slices: roles of intracellular Ca2+ and glycolysis. Brain Res. *780*, 86–94. https://doi.org/10.1016/S0006-8993(97)01149-9.

63. Meech, R.W., and Thomas, R.C. (1977). The effect of calcium injection on the intracellular sodium and pH of snail neurones. J. Physiol. *265*, 867–879.

64. Schwiening, C.J., Kennedy, H.J., and Thomas, R.C. (1993). Calcium-hydrogen exchange by the plasma membrane Ca-ATPase of voltage-clamped snail neurons. Proc. Biol. Sci. *253*, 285–289.

65. Makani, S., and Chesler, M. (2010). Rapid rise of extracellular pH evoked by neural activity is generated by the plasma membrane calcium ATPase. J. Neurophysiol. *103*, 667–676. https://doi.org/10.1152/jn.00948.2009.

66. Kaila, K., Paalasmaa, P., Taira, T., and Voipio, J. (1992). pH transients due to monosynaptic activation of GABAA receptors in rat hippocampal slices. Neuroreport *3*, 105–108.

67. Dixon, D.B., Takahashi, K., and Copenhagen, D.R. (1993). L-glutamate suppresses HVA calcium current in catfish horizontal cells by raising intracellular proton concentration. Neuron *11*, 267–277.

68. Takahashi, K.-I., and Copenhagen, D.R. (1996). Modulation of neuronal function by intracellular pH. Neurosci. Res. *24*, 109–116. https://doi.org/10.1016/0168-0102(95)00989-2.

69. Tombaugh, G.C., and Somjen, G.G. (1997). Differential sensitivity to intracellular pH among high- and low-threshold Ca2+ currents in isolated rat CA1 neurons. J. Neurophysiol. *77*, 639–653. https://doi.org/10.1152/jn.1997.77.2.639.

70. Willoughby, D., Thomas, R., and Schwiening, C. (2001). The effects of intracellular pH changes on resting cytosolic calcium in voltage-clamped snail neurones. J. Physiol. *530*, 405–416. https://doi.org/10.1111/j.1469-7793.2001.0405k.x.

71. Szydlowska, K., and Tymianski, M. (2010). Calcium, ischemia and excitotoxicity. Cell Calcium *47*, 122–129. https://doi.org/10.1016/j.ceca.2010.01.003.

72. Kann, O., Papageorgiou, I.E., and Draguhn, A. (2014). Highly energized inhibitory interneurons are a central element for information processing in cortical networks. J. Cereb. Blood Flow Metab. *34*, 1270–1282. https://doi.org/10.1038/jcbfm.2014.104.

73. Gutiérrez, R., and Heinemann, U. (1999). Synaptic reorganization in explanted cultures of rat hippocampus. Brain Res. *815*, 304–316.

74. Bausch, S.B., and McNamara, J.O. (2000). Synaptic connections from multiple subfields contribute to granule cell hyperexcitability in hippocampal slice cultures. J. Neurophysiol. *84*, 2918–2932. https://doi.org/10.1152/jn.2000.84.6.2918.

75. Tauck, D.L., and Nadler, J.V. (1985). Evidence of functional mossy fiber sprouting in hippocampal formation of kainic acid-treated rats. J. Neurosci. *5*, 1016–1022.

76. Babb, T.L., Kupfer, W.R., Pretorius, J.K., Crandall, P.H., and Levesque, M.F. (1991). Synaptic reorganization by mossy fibers in human epileptic fascia dentata. Neuroscience *42*, 351–363. https://doi.org/10.1016/0306-4522(91)90380-7.

77. Isokawa, M., Levesque, M.F., Babb, T.L., and Engel, J. (1993). Single mossy fiber axonal systems of human dentate granule cells studied in hippocampal slices from patients with temporal lobe epilepsy. J. Neurosci. *13*, 1511–1522.

78. Stoppini, L., Buchs, P.-A., and Muller, D. (1991). A simple method for organotypic cultures of nervous tissue. J. Neurosci. Methods *37*, 173–182. https://doi.org/10.1016/0165-0270(91)90128-M.

STAR★METHODS

KEY RESOURCES TABLE

REAGENT or RESOURCE	SOURCE	IDENTIFIER
Bacterial and Virus Strains		
AAV8-EF1a-double floxed-ClopHensorN-WPRE-HGHpA	The Vector Core at the University of North Carolina at Chapel Hill (*UNC Vector Core*)	AAV custom production using this paper's floxed ClopHensorN plasmid made available on Addgene Cat#193728
Chemicals, Peptides, and Recombinant Proteins		
Earle's Balanced Salt Solution with $CaCl_2$ and $MgSO_4$	Thermo Fisher Scientific	Cat#24010043
Millicell-CM membranes	Sigma-Aldrich (USA)	Cat#PICM03050
Minimum Essential Media with GlutaMAX-I	Thermo Fisher Scientific	Cat#41090036
Heat-inactivated horse serum	Thermo Fisher Scientific	Cat#26050088
B27 supplement	Thermo Fisher Scientific	Cat#17504044
Nigericin	Sigma-Aldrich (USA)	Cat#N7143
Tributyltin chloride	Sigma-Aldrich (USA)	Cat#T50202
Chloride ionophore I	Sigma-Aldrich (USA)	Cat#99408-0.1 ML-F
Experimental Models: Cell Lines		
HEK293 cells	Sigma-Aldrich (USA)	Cat#85120602
Experimental Models: Organisms/Strains		
Mouse: PV-Cre: B6; 129P2-Pvalb$^{tm1(cre)Arbr}$/J	The Jackson Laboratory (USA)	RRID:IMSR_JAX:008069
Mouse: SST-IRES-Cre: Sst$^{tm2.1(cre)Zjh}$/J	The Jackson Laboratory (USA)	RRID:IMSR_JAX:013044
Mouse: VIP-IRES-Cre: Vip$^{tm1(cre)Zjh}$/J	The Jackson Laboratory (USA)	RRID:IMSR_JAX:010908
Mouse: CamK2a-Cre: Tg(Camk2a-cre)T29-1Stl/J	The Jackson Laboratory (USA)	RRID:IMSR_JAX:005359
Mouse: C57BL/6J: C57BL/6J	The Jackson Laboratory (USA)	RRID:IMSR_JAX:000664
Recombinant DNA		
ClopHensorN plasmid	Addgene	Cat#50758
floxed ClopHensorN plasmid	Addgene	Cat#193728
Software and Algorithms		
MATLAB	Mathworks (USA)	R2017b
GraphPad Prism	GraphPad Software (USA)	v6.01
CorelDraw	Corel Corporation (USA)	X6

RESOURCE AVAILABILITY

Lead contact

Further information and requests for resources and reagents should be directed to and will be fulfilled by the lead contact, Colin J. Akerman (colin.akerman@pharm.ox.ac.uk).

Materials availability

The plasmid generated in this study has been deposited to Addgene (https://www.addgene.org) as plasmid # 193728.

Data and code availability

- All data reported in this paper will be shared by the lead contact upon request.

- This paper does not report original code.

- Any additional information required to reanalyze the data reported in this paper is available from the lead contact upon request.

EXPERIMENTAL MODEL AND SUBJECT DETAILS

Preparation of organotypic hippocampal brain slices

All animal work was carried out in accordance with the Animals (Scientific Procedures) Act, 1986 (UK). Organotypic hippocampal brain slices, referred to as 'brain slices' or 'slices', were prepared from 5 to 7 day-old male and female transgenic mice,[78] and matured in culture for 3 weeks before being used for experiments. Slices from both sexes contributed to each experimental condition. Previous work has established that hippocampal organotypic slices retain fundamental features of the hippocampal circuit, including appropriate distributions of interneurons and distinct subcellular targeting of pyramidal neurons.[34,36–38] At the stages studied here, glutamatergic and GABAergic synaptic transmission, including chloride homeostasis, have been shown to be mature.[36,37,45] Mice were either heterozygous or homozygous PV-Cre mice (B6; 129P2-Pvalb$^{tm1(cre)Arbr}$/J), SST-IRES-Cre mice (Sst$^{tm2.1(cre)Zjh}$/J), VIP-IRES-Cre mice (Vip$^{tm1(cre)Zjh}$/J), or CamK2a-Cre mice (Tg(Camk2a-cre)T29-1Stl/J) purchased from The Jackson Laboratory (USA). We did not observe differences in expression levels when delivering floxed ClopHensorN to slices from heterozygous or homozygous mice. Heterozygous mice were produced by crossing homozygous animals of the above Cre-expressing lines with C57BL/6J mice.

All reagents were purchased from Sigma-Aldrich (USA), unless stated otherwise. The whole brain was extracted and transferred into cold (4°C) dissection media containing Earle's Balanced Salt Solution with $CaCl_2$ and $MgSO_4$ (Thermo Fisher Scientific, UK), supplemented with 25.5 mM HEPES, 36.5 mM D-glucose and 5 mM NaOH. The hemispheres were separated, and the individual hippocampi were dissected and immediately sectioned into 400-μm-thick slices on a McIlwain tissue chopper (Mickle, UK). Slices from the middle (anterior-posterior) region of the hippocampus with clearly intact architecture were selected, and cold dissection media was then used to rinse slices before placing the slices onto sterile, porous Millicell-CM membranes. Slices were maintained in media containing 78.8% (v/v) Minimum Essential Media with GlutaMAX-I (Thermo Fisher Scientific), 20% (v/v) heat-inactivated horse serum (Thermo Fisher Scientific), 1% (v/v) B27 (Thermo Fisher Scientific), 30 mM HEPES, 26 mM D-glucose, 5.8 mM $NaHCO_3$, 1 mM $CaCl_2$, 2 mM $MgSO_4 \cdot 7H_2O$. Brain slices were incubated at 35.5–36°C in a 5% CO_2 humidified incubator.

METHOD DETAILS

Generating the floxed ClopHensorN construct

Floxed ClopHensorN was generated by subcloning the inverted sequence of ClopHensorN into the backbone of a double-floxed plasmid called 'pAAV-EF1a-double floxed-hChR2(H134R)-mCherry-WPRE-HGHpA', which was a gift from Karl Deisseroth (Addgene plasmid # 20297; https://www.addgene.org/20297; RRID:Addgene_20297). The resulting floxed ClopHensorN was under the control of an elongation factor 1α (EF-1α) promoter, a Woodchuck hepatitis virus posttranscriptional regulatory element (WPRE), and a polyadenylation termination sequence. The 22 amino acid linker from the original ClopHensor construct was maintained.[26] We called the resulting construct 'pAAV-EF1a-double floxed-ClopHensorN-WPRE-HGHpA' and have made this floxed version of ClopHensorN available to the scientific community via Addgene (https://www.addgene.org) as plasmid # 193728. High titer adeno-associated virus (AAV; ~10^{12} IU/mL) was then made by packaging the floxed ClopHensorN construct into AAV serotype 8 at the University of North Carolina Gene Therapy Center Vector Core (USA).

Viral transduction of brain slices

Organotypic hippocampal brain slices afford efficient delivery of genetic constructs via visually guided AAV injections. Brain slices were transduced after 3–5 days in culture by injecting AAV particles (mixed with 1% w/v fast green for visualization) into 5–10 locations along the pyramidal cell layer of the hippocampus, to deliver ~250 nL per slice. Fine injection pipettes were pulled from glass capillaries (1.2 mm outer diameter, 0.69 mm inner diameter; Warner Instruments) using a horizontal puller (Sutter P-97, USA). Pipettes were mounted on a manual manipulator (Narishige, Japan) and monitored under a microscope (Leica S6E, Germany) coupled with an external fiber optic light source (Photonic Leica CLS 100X, Germany). A Picospritzer II system (General Valve, Germany) delivered controlled pressure pulses (5-to-10 psi for 1 s) to facilitate slow diffusion of the viral solution into the tissue. Previous work established that this transduction protocol

produces good specificity and efficiency in targeting different Cre-expressing interneuron populations.[34] Feeding media was supplemented with 1% (v/v) antibiotic and antimycotic solution (with 10,000 units penicillin, 10 mg streptomycin and 25 μg amphotericin B per mL) for up to two feeding sessions after injection.

Electrophysiological recordings and epileptiform activity

Brain slices were gently transferred to a submerged recording chamber by cutting and handling the porous membrane to which the slice was attached. The slice was stabilized by attaching the membrane to the recording chamber using glisseal. The chamber was continuously superfused with artificial cerebrospinal fluid (aCSF) containing (in mM): NaCl (120), KCl (3), $MgCl_2$ (0–1.5), $CaCl_2$ (2-to-3), NaH_2PO_4 (1.2), $NaHCO_3$ (23), D-glucose (11) and ascorbic acid (0.2) and maintained at 28°C. Osmolarity was adjusted to 290 mOsm and pH was adjusted to 7.36 with NaOH. Oxygen and pH levels were stabilized by bubbling the aCSF with 95% O_2 and 5% CO_2. At this stage, slices were approximately 200-250 μm thick and confirmed as having clear architecture (dentate gyrus, defined pyramidal neuron layer extending from CA1 to CA3), with neurons at the surface of the slice. Neurons were visualized under transmitted or epifluorescence light using 10× and 60× water-immersion microscope objectives and appropriate filter cubes (Olympus BX51WI, Japan) and targeted for single or dual-patch whole-cell recordings. Patch pipettes of 4–9 MΩ tip resistance were pulled from filamental borosilicate glass capillaries with an outer diameter of 1.2 mm and an inner diameter of 0.69 mm (Warner Instruments, USA), using a horizontal puller (Sutter P-97, USA), and filled with a K-gluconate internal solution (134 mM K-gluconate, 2 mM NaCl, 10 mM HEPES, 2 mM Na_2ATP, 0.3 mM NaGTP, 2 mM MgATP), which had been prepared to a pH of 7.36 using KOH, and an osmolarity of 290 mOsm. Before use, internal solution was filtered with a 0.22 μm syringe filter (Merck Millipore, USA). Pipettes were mounted to a headstage (CV-7b, Molecular Devices, USA) and controlled via a Multiclamp 700B amplifier (Molecular Devices, USA). Recordings were low-pass filtered online at 2 kHz (8-pole Bessel), acquired using Clampex software (pClamp 10, Molecular Devices, USA), and exported into MATLAB (R2017a, Mathworks, USA) for offline analysis using custom scripts.

Organotypic hippocampal brain slices have been used as an experimentally accessible model of temporal lobe epilepsy because when maintained in culture, the slices exhibit EDs, reminiscent of epileptogenesis in post-traumatic epilepsy.[33,49] EDs were detected via membrane potential recordings from pyramidal neurons, and recordings typically lasted ~30 min in order to acquire simultaneous imaging and electrophysiological data across multiple EDs. The EDs were characterized as large ictal-like discharges, interspersed by periods of relative network quiescence, with no evidence of interictal-like activity. The median duration of EDs was 79.51 s (IQR [35.94 to 218.31]), and the median ED frequency was 5.44 events/hour (IQR [2.3 to 17.06]). Baseline measurements were made during quiescent periods where there were no EDs. An automated detection algorithm was used to identify the start and end of individual EDs. Traces were downsampled to 1 kHz and then band-pass filtered (typically 0.05-to-0.2 Hz) using a Bessel filter (second order). The signal was corrected for the rise time of the filter and then rectified, thresholded and binarized.

ClopHensorN imaging of intracellular chloride and pH

All ClopHensorN imaging and calibration was performed using a Zeiss LSM 880 confocal microscope, via a 20× water-immersion objective (W Plan-Apochromat, NA 1.0), and controlled via ZEN software (Zeiss). ClopHensorN was used as a ratiometric probe and excited at 561 nm using a diode-pumped solid-state laser, and at 458 nm and 488 nm using separate lines of the same argon laser. When exciting ClopHensorN at 561 nm, emitted fluorescence was collected by a photomultiplier tube (PMT) in the 635–700 nm range. When exciting ClopHensorN at 458 nm and 488 nm, emitted fluorescence was collected by a high sensitivity gallium arsenide phosphide PMT (GaAsP-PMT) in the 500–550 nm range. ClopHensorN is a fusion protein comprising the pH and chloride sensitive E^2GFP, which is linked to the pH and chloride insensitive tdTomato.[26,27] E^2GFP has an isosbestic point for pH at 458 nm, meaning that emission is stable regardless of pH.[26] By applying the calibration curves in Figure 2, the ratio of emitted fluorescence under 458 nm and 561 nm excitation was used to estimate chloride concentration, and the ratio of emitted fluorescence under 488 nm and 458 nm excitation was used to measure pH.[26,27] Optical zoom was used so typically only one ClopHensorN-expressing neuron was located within the field of view and the soma was maintained at the same focal plane for the duration of the recording. Fluorescence was always collected over the soma and background fluorescence was subtracted. Data was then exported and processed using custom MATLAB scripts. Under- and over-exposure thresholds were used to exclude regions that had low signal-to-noise ratio, or were overexposed. This ensured comparable levels of ClopHensorN expression across the different neuronal populations. Bleaching correction was performed separately for

each wavelength by fitting exponential decay or polynomial functions to approximate the bleaching rate. Following bleaching correction, the pH (F_{488}/F_{458}) and chloride (F_{458}/F_{561}) ratios were calculated and used to infer the pH and chloride concentration according to the calibration curves. pH ratios were considered if they fell within the range of the pH calibration curve. Chloride ratios were included if they were above the minimum ratio of the chloride calibration curve range for the corresponding inferred pH.

ClopHensorN calibration

ClopHensorN calibration was performed as previously described[26,27,43] using HEK293 cells expressing ClopHensorN (Addgene plasmid # 50758), which enabled us to make rapid extracellular solution changes. Intracellular and extracellular pH and chloride concentration were equilibrated by using an ionophore cocktail comprising the K^+/H^+ exchanger nigericin (20 μM), the Cl^-/OH^- exchanger tributyltin chloride (40 μM), and the chloride ionophore I (1 μM), in high-K^+ solutions of varying Cl^- concentration and pH. Cl^- concentration was varied by mixing different proportions of two high-K^+ solutions (in mM): (i) KCl (143), $CaCl_2$ (2), $MgCl_2$ (4), HEPES free acid (20), D-glucose (10), NaH_2PO_4 (1.2), and (ii) K-gluconate (143), Ca-gluconate (2), $MgSO_4$ (4), HEPES free acid (20), D-glucose (10), NaH_2PO_4 (1.2). Separate calibration curves were obtained by monitoring the pH and chloride ratios while systematically changing the extracellular pH or chloride concentration. As the calibration uses averaged measurements from cell populations, individual estimates of intracellular chloride concentration can exhibit negative values. To calibrate for pH, the intracellular pH was controlled by titrating KOH or HNO_3 to the HEPES-based buffer solution containing the ionophore cocktail described above. Following each pH adjustment, the intracellular and extracellular compartments were left to equilibrate for at least 15 min before imaging ClopHensorN. According to the Grynkiewicz equation,[44] the formation of a 1:1 proton:ClopHensorN complex would lead to the following relationship:

$$pH_i = pK_a + \log\left(\frac{R_{pH} - R_A}{R_B - R_{pH}}\right) + \log\left(\frac{F_{458,A}}{F_{458,B}}\right)$$

Where pH_i is intracellular pH, pK_a is the acid dissociation constant of ClopHensorN, R_{pH} is the pH ratio, R_A and R_B are the pH ratios for ClopHensorN in the most acidic and basic conditions, respectively, and $F_{458,A}$ and $F_{458,B}$ represent the fluorescence of ClopHensorN when excited at 458 nm in its most acidic and basic form, respectively. Given that the fluorescence of E^2GFP does not change with pH when the fluorophore is excited at 458 nm, the equation above can be simplified:

$$pH_i = pK_a + \log\left(\frac{R_{pH} - R_A}{R_B - R_{pH}}\right)$$

The calibration data were then fitted using this rearranged equation:

$$R_{pH} = \frac{R_B \times 10^{pH - pK_a} + R_A}{1 + 10^{pH - pK_a}}$$

For fitting this equation, the pH ratio data within one standard deviation of the mode for each pH value was used. This allowed for pK_a, R_A and R_B to be calculated. To calibrate for chloride, the intracellular chloride concentration was controlled by systematically adjusting the extracellular pH and chloride concentration, which was changed by using KCl to replace potassium gluconate from the HEPES-based buffer solution containing the ionophore cocktail. According to the Grynkiewicz equation, the formation of a 1:1 chloride-ClopHensorN complex would result in the following relationship:

$$[Cl^-]_i = K_d^{Cl^-}[pH_i] \times \left(\frac{R_{Cl^-} - R_{free}}{R_{bound}[pH_i] - R_{Cl^-}}\right) \times \left(\frac{F_{561,free}}{F_{561,bound}}\right)$$

In this equation, $[Cl^-]_i$ is the intracellular chloride concentration, $K_d^{Cl^-}[pH_i]$ is the chloride dissociation constant that depends on pH, R_{Cl^-} is the chloride ratio, R_{free} is the chloride ratio of ClopHensorN in its chloride-free form, $R_{bound}[pH_i]$ is the chloride ratio of ClopHensorN in its chloride-bound form and $F_{561,free}$ and $F_{561,bound}$ represent the fluorescence of ClopHensorN when excited at 561 nm in its chloride-free and chloride-bound form, respectively. Given the fluorescence of tdTomato does not change with pH or chloride when the fluorophore is excited at 561 nm, the equation above can be simplified as:

$$[Cl^-]_i = K_d^{Cl^-}[pH_i] \times \left(\frac{R_{Cl^-} - R_{free}}{R_{bound}[pH_i] - R_{Cl^-}}\right)$$

The calibration data were then fitted using the following rearranged equation:

$$R_{Cl^-} = \frac{[Cl^-]_i \times R_{bound}[pH_i] + K_d^{Cl^-}[pH_i] \times R_{free}}{K_d^{Cl^-}[pH_i] + [Cl^-]_i}$$

Separate chloride calibrations were performed at different pH values, which allowed the calculation of $K_d^{Cl^-}[pH_i]$, R_{free} and $R_{bound}[pH_i]$. $R_{bound}[pH_i]$ was assumed to relate linearly with pH, and $K_d^{Cl^-}[pH_i]$ relates with pH according to the relationship shown below:

$$K_d^{Cl^-}[pH_i] = {}^1K_d^{Cl^-} \times \left(\frac{1 + 10^{pK_a - pH_i}}{10^{pK_a - pH_i}}\right)$$

${}^1K_d^{Cl^-}$ represents the dissociation constant for chloride in the fully protonated form of ClopHensorN.

QUANTIFICATION AND STATISTICAL ANALYSIS

Digital signal processing and data presentation were performed using custom scripts in the MATLAB environment (R2017b, Mathworks, USA). Figures were built using vector-based graphic design in CorelDraw (X6, Corel Corporation, USA) and the statistical software GraphPad Prism (v6.01, GraphPad Software, USA). Statistical tests are reported at the relevant points in the text, along with the number of observations for each experiment, the test statistic, degrees of freedom, and the p value (GraphPad Prism; MATLAB). Non-parametric tests were used when the data were not normally distributed. Appropriate post-hoc tests were used when ANOVA tests confirmed a statistically significant effect. Pearson correlations were used to determine the degree of correlation between the membrane potentials of pairs of neurons.